Solution and Solid-State Study of the Spin-Crossover [Fe II (R-bik) 3](BF 4) 2 Complexes (R = Me, Et, Vinyl)

Siddhartha De, Subrata Tewary, Delphine Garnier, Yanling Li, Geoffrey Gontard, Laurent Lisnard, Alexandrine Flambard, Frank Breher, Marie-Laure Boillot, Gopalan Rajaraman, et al.

Solution and Solid-State Study of the Spin-Crossover $[Fe^{II}(R\text{-}bik)_3](BF_4)_2$ complexes [R = Me, Et, Vinyl]

Siddhartha De,[a] Subrata Tewary,[b] Delphine Garnier,[a],[c] Yanling Li,[a] Geoffrey Gontard,[a] Laurent Lisnard,[a] Alexandrine Flambard,[a] Frank Breher,[c] Marie-Laure Boillot,[d] Gopalan Rajaraman,[b]* and Rodrigue Lescouëzec[a]*

Abstract: The magnetic properties of three spin-crossover complexes, $[Fe^{II}(R\text{-}bik)_3](BF_4)_2.nH_2O$ (**1-3**), based on bis-imidazolyl-ketone ligands were investigated in solution and solid-state. Their properties were compared with those of the ketone-free analogue, $[Fe^{II}(bim)_3](OTf)_2$ (**4**). The alkyl and vinyl R groups have weak influence on the transition temperature, $T_{1/2}$, in solution while stronger differences are observed in solid-state because different intermolecular interactions occur in **1-3**. The spin-state equilibria in solution were followed by SQUID magnetometry and Evans' NMR method. Interestingly, the equilibria can also be simply and efficiently probed by following the temperature dependence of an adequately chosen ^{1}H chemical shift. Overall these experiments give coherent results with $T_{1/2}$ located between 320 and 335 K, a narrow range in comparison to the solid-state. DFT calculations allowed rationalizing the differences in the magnetic differences. The molecular orbital and spin density calculations reveal that the presence of the C=O group between the imidazolyl units in the ligands of **1**-**3** leads to an extended aromatic system, an effective π-acceptor effect, stabilizing a LS state and reducing the LS-HS gap in comparison to **4**.

Introduction

Spin-crossover (SCO) complexes have been the focus of considerable interest for both fundamental and practical reasons. These complexes, whose electronic properties can be reversibly switched by external stimuli (light, temperature, pressure, etc.), are interesting building blocks to design responsive molecular materials. For instance, they appear as good candidates for the development of molecular-based sensors,[1] logic gates,[2] memories[3] and display devices.[4]

[a] Dr. S. De, Dr. D. Garnier, Dr. Y. Li, G. Gontard, Dr. L. Lisnard, Dr. A. Flambard, Prof. R. Lescouëzec
Institut Parisien de Chimie Moléculaire, (UMR 8232),
Université Paris 06, Sorbonne Universités, 4 place Jussieu, 75252 Paris cedex 5, France.
rodrigue.lescouezec@upmc.fr
[b] S. Tewary, Dr. G. Rajaraman
Department of Chemistry,
Indian Institute of Technology Bombay, Powai, Mumbai 400 076, Maharashtra, India.
rajaraman@chem.iitb.ac.in
[c] Dr. D. Garnier, Prof. F. Breher
Institut für Anorganische Chemie,
Karlsruhe Institut für Technologie (KIT), Campus Süd, Engesserstr. 15, Geb. 30.45, D-76131 Karlsruhe, Germany
[d] Dr. M. L. Boillot
Institut de Chimie Moléculaire et des Matériaux d'Orsay,
Univ. Paris Sud, Université Paris-Saclay, CNRS, 91405 Orsay, cedex, France

The Fe^{II} SCO complexes represent the largest family of SCO complexes, many of them exhibiting an octahedral $\{N_6\}$ coordination polyhedron. In these complexes, the diamagnetic LS configuration (t_{2g}^6, S = 0) is converted into a paramagnetic HS one ($t_{2g}^4e_g^2$, S = 2). The spin-state switching is associated to significant changes in magnetic or optical properties and the process can thus be followed by magnetometry, optical studies or any other technique. The temperature dependence of the physical values related to the spin state of the molecules allows the determination of the relative amount of HS and LS fractions. These data can thus be used to extract the thermodynamic parameters associated to the SCO, in particular the entropic and enthalpic contributions to the spin-equilibrium.[5-7] The NMR spectroscopy represents an other useful tool to follow the spin-equilibrium in solution and to determine its associated thermodynamic parameters. The Evans method, which gives an indirect access to the magnetic susceptibility of paramagnetic compounds in solution and allows the extraction of the relative amount of the HS fraction, γ_{HS}, is the most common approach.[6] However, this method often suffers from errors, arising for example from the approximations on the paramagnetic solute concentration or from the presence of paramagnetic impurities. As reported by A. Walker *et al.* the temperature dependence of selected ^{1}H chemical shifts can alternatively be used to investigate spin-crossover equilibria.[7a] This approach have been used in various recent studies of Fe^{II} SCO complexes.[7b-d] In fact, the NMR chemical shifts are highly sensitive to changes in electronic ground states in transition metal complexes.[8] Alternatively, magnetic measurements of solutions can be used to follow the temperature dependence of the magnetic susceptibility in a direct manner.[9] However, this method is not so common and it may suffer from approximations, due to an important diamagnetic contribution for example (due to the dilution of the paramagnetic species in a diamagnetic solvent). During the last few years, a number of switchable polynuclear complexes featuring derivatives of the bis(1-R-imidazol-2-yl)ketone ligand, R-bik, have been investigated by some of us (R being a methyl or a vinyl group).[10, 11] Cyanide-bridged polynuclear complexes in which the $\{M(R\text{-}bik)_2(NC)_2\}$ subunit exhibits a spin transition (when M = Fe) that can be associated to a metal-metal electron transfer (when M = Co) have been reported. In these systems, the switchable properties in the solid-state depend on the nature of the ligands but also on various parameters that can be difficult to control (nature of the crystal phase, presence of solvate molecules in the crystal lattice, intermolecular interactions). In the present work, we chose to focus our study on the mononuclear Fe^{II} complexes of molecular formula $[Fe(R\text{-}bik)_3](BF_4)_2.n(H_2O)$ (Me-bik = bis(1-methylimidazol-2-yl)ketone (**1**), Et-bik = bis(1-ethylimidazol-2-

yl)ketone (**2**) and V-bik = bis(1-vinylimidazol-2-yl)ketone (**3**); n= 0.25 (**1**), 0 (**2**) and 1.5 (**3**)) and the paramagnetic derivative $[Fe^{II}(bim)_3](OTf)_2$ (**4**) (bim = bis(1-methylimidazol-2-yl)methane). The $[Fe(R\text{-}bik)_3]^{2+}$ tris-chelate complexes are reminiscent of the well-known low-spin $[Fe(phen)_3]^{2+}$ and $[Fe(bipy)_3]^{2+}$ complexes where 2,2'-bipyridine and 1,10-phenanthroline are the α-diimine ligands.[12,13] However, in the present case the β-diimine ligands, R-bik, form six-membered rings that induce weaker ligand field on the Fe^{II} ion, and in some cases, spin-crossover phenomenon.

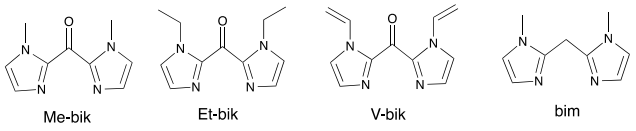

Scheme 1. Bis-imidazolyl chelate ligands used in this work.

Our purpose is to investigate how slight changes in this ligand family can affect the switchable properties of the complexes in solution. More specifically, in this contribution we have investigated the spin equilibria in solution by using variable temperature (VT) ^{1}H NMR and compared the results with Evans NMR method and solution SQUID magnetometry. We have also confronted these results to those obtained in solid-state. Besides, DFT calculations have been performed on the different complexes to probe their electronic structure and rationalize their properties.

Results and Discussion

Solid-state measurements

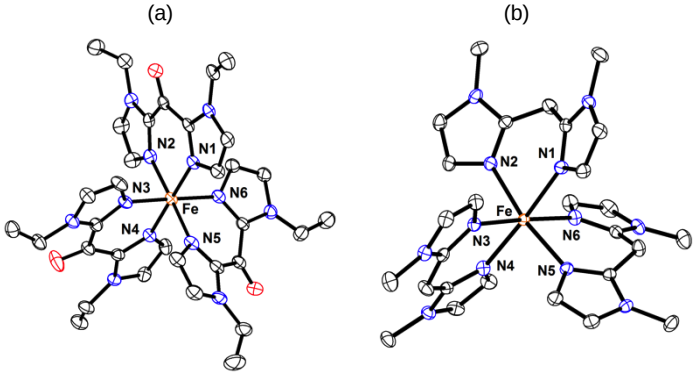

Figure 1. Perspective view (Ortep) of the $[Fe^{II}(V\text{-}bik)_3]^{2+}$ (a) and $[Fe^{II}(bim)_3]^{2+}$ (b) cations at 200 K in **3** and **4** respectively, together with the atom numbering of their coordination sphere. All hydrogen atoms and counter-anions have been omitted for clarity.

Complexes **1-4** were isolated as dark blue plate-like crystals (**1-3**) or colourless needle-like crystals (**4**) from the reaction of Fe^{II} salts with three equivalents of the bis-imidazolyl chelate ligands.

Table 1. Space groups and cell-parameters of **1-4** measured at 200 K.

Compounds:	**1**	**2**	**3**	**4**
Space group	Pbca	C2/c	P-1	$P2_1/c$
a (Å)	15.3604 (3)	21.1447 (5)	9.3631 (2)	20.5632(5)
b (Å)	11.6415 (3)	16.0717 (4)	11.4700 (3)	11.3824(3)
c (Å)	37.4475 (7)	12.7572 (3)	18.6414 (4)	16.2092(4)
c (Å)	37.4475 (7)	12.7572 (3)	18.6414 (4)	16.2092(4)
α (°)	90	90	99.121 (2)	90
β (°)	90	114.657 (1)	93.443 (2)	90.047(1)
γ (°)	90	90	90.240 (1)	90

Cell parameters and space groups are given in table 1. Their structures (determined at 200 K) consist of tris-chelate $[Fe^{II}(L)_3]^{2+}$ cationic units (L = R-bik or bim), tetrafluoroborate (**1-3**) or triflate (**4**) counter anions and water solvent molecule. In the case of **3,** it was not possible to accurately define the exact position of the crystallization water molecules. As the BF_4^- is disordered over two positions, with a relative occupancy of 1/2, we assume the other position is filled by water. Perspective views of the cationic trischelate complexes are shown in Figure 1 (**3-4**) and in Figure S1 (**1-2**) and selected bond lengths and angles are given in Table 2. In the four complexes, the Fe^{II} ions adopt an octahedral $\{N_6\}$ coordination sphere made of three *N,N*-chelate-bonded ligands. The Fe-N bond lengths in **1-3** are close to each other and in the range: 1.983(2) - 2.008(2) Å (**1**), 1.989(2) - 2.005(2) Å (**2**) and 1.977(3) - 1.995(3) Å (**3**). In the three complexes, the average Fe-N distance of *ca.* 1.99 Å is in agreement with the occurrence of a iron(II) low-spin state at 200 K.[14] In contrast, the Fe-N bond lengths in **4** are significantly higher and range from 2.163(3) to 2.207(3) Å (av. 2.18 Å). These values are coherent with a Fe^{II} high-spin state. It is worth noticing that other crystal structures with the $[Fe^{II}(Me\text{-}bik)_3]^{2+}$ cation have already been reported with other counter anions.[15] The crystal structure of $[Fe(Me\text{-}bik)_3](ClO_4)_2$ measured at 298 K reveals a high-spin Fe^{II} compound with an average Fe-N distance of 2.14 Å, whereas the crystal structures of the complexes $[Fe(Me\text{-}bik)_3]Cl_2$ and $[Fe(Me\text{-}bik)_3](OTf)_2$ determined at 150 K exhibit an average Fe-N distances of 1.98 Å that matches well with the distances encountered in **1-3**.[14b,14c] The β-diimine ligands form six-membered chelate rings that exhibit average bite angles of 89.1(5)° (**1**), 89.7(4)° (**2**), 88.9(9)° (**3**) and 84.2(5)° (**4**). The values found in **1-3** are closer to orthogonality than those of other LS Fe^{II} complexes made of α-diimine ligands with five-membered chelate ring, such as the well known LS $[Fe^{II}(phen)_3]^{2+}$ complex (with bite angles of *ca.* 82.8°).[12b] The sum of the deviation from orthogonality of the twelve *cis*-N-Fe-N angles (noted Σ)[16] is relatively low in **1-3** (respectively: 13.5(4)°, 8.9(3)° and 21.2(5)°) and indicate a moderate distortion of the octahedral coordination sphere. In contrast this value reaches Σ = 47.6°, within the related LS $[Fe(phen)_3]^{2+}$ complex. The Σ values in **1-3** are also significantly lower than the one measured

in the HS $[Fe(bim)_3]^{2+}$ (Σ = 42.4(5)°). The continuous shape measure analysis (CShM),[17,18] allows a more precise quantification of the deviation of the coordination spheres from an ideal geometry. The distorsion of the coordination sphere reflects the spin state of the Fe^{II} ion: in the present case, very small values of the shape factor[16,17] are observed in **1-3** (table 2), indicating an almost perfect octahedral surrounding, whereas a higher one is obtained in **4**, as expected for a HS Fe^{II} complex. The bim and R-bik β-diimine ligands exhibit dihedral angles between imidazole rings, which can vary significantly from one ligand to another within the same complex: 4.03(10)°, 9.03(9)° and 11.54(9)° (**1**); 10.35(8)°, 10.35(8)° and 13.02(7)° (**2**); 2.08(15), 10.77(13)° and 21.79(15)° (**3**); 11.87(16)°, 27.29(14)° and 34.23(15)° (**4**). The three complexes **1-3** exhibit the same average C=O bond length, which amounts to 1.22(1) Å, however, significant differences in Fe-C-O angles are observed for the three compounds. While the Fe-C-O angle approaches linearity for **1** (ranging from 173.2(2)° to 178.1(3)°) and **2** (from 177.0(2)° to 180°), they deviate significantly from 180° in **3** (from 160.5(3)° to 169.8(4)°). Overall these data show that these β-diimine ligands are more flexible than the α–diimine ligands such as the 1,10-phenanthroline.

Table 2. Structural data related to the geometry of the coordination sphere in **1-4**.

Compounds:	**1**	**2**	**3**	**4**
Temperature	200 K	200 K	200 K	200 K
d[Fe-N(L)]$_{av}$	1.997(11) Å	1.997(9) Å	1.987(8) Å	2.181(19) Å
Bite (N-Fe-N)$_{av}$ angle	89.1(5)°	89.7(4)°	88.9(9)°	84.2(5)°
$\sum_{1}^{12} \lvert 90 - a \rvert$	13.5(4)°	8.9(3)°	21.2(5)°	42.4(5)°
trans(N-Fe-N)$_{av}$ angle	178.0(4)°	178.4(6)°	177.6(14)°	174.8(38)°
Dihedral angles*	4.03(10)° 9.03(9) 11.54(9)°	10.35(8)° 10.35(8)° 13.02(7)°	2.08(15)° 10.77(13)° 21.79(15)°	11.87(16)° 27.29(14)° 34.23(15)°
Shape factor *S* (OC-6) [a]	0.042	0.019	0.063	0.314

[a] See text for details.

Finally there are no important intermolecular interaction in **1**-**4**, neither strong hydrogen bonding, nor π–π interaction. However short contacts (with interatomic distances shorter than the sum of the van der Waals radii) are found between C-H groups from methyl and ethyl substituants and perpendicularly oriented imidazol ring planes. Thus the crystal packing of these complexes is most probably influenced by these CH•••π interactions between imidazolyl ring and alkyl proton. Such a CH•••π interaction is often referred to as a point-to-face or T-shaped arrangement[19] and their energy lie in the range of 1-2 kJ/mol.[20] In **1** and **2** the average distance of CH•••C(π) contacts are 2.78 and 2.77 Å, respectively. These distances are quite significant as they lie at the middle of the accepted distance range for such supramolecular interaction (from 2.6 to 3.1 Å).[21] The amplitude of these interactions are also described by the intermolecular CH•••ring-centroid distance, which amounts to 2.65 Å in **1** and 2.67 Å in **2** for the shortest contact. The interaction is much more important in **2** although both values remain within the accepted range.[20] The CH•••C(π) / CH•••ring-centroid interactions are also more prominent in **2** as they involve pairs of interactions running along the z axis: two of the Et-Im groups of a same Et-bik ligand acting simultaneously as donor and acceptor (Figure 2)**.** In compound **3** and **4** no significant intermolecular CH•••C(π) / CH•••ring-centroid short interactions (less than sum of C-H van der Waals radii) are found.

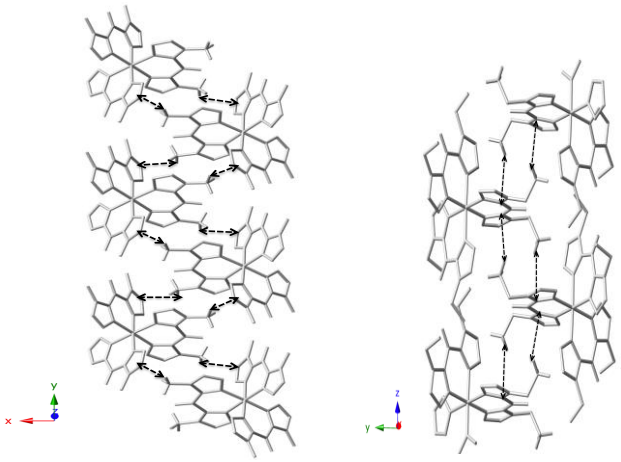

Figure 2. View of the intermolecular C-H•••π interactions (black dotted lines) between adjacent complexes in **1** (left) and **2** (right); H atoms not involved in interactions have been omitted for clarity**.**

Magnetic properties in the solid state

The $\chi_M T$ *vs* T curves for **1**-**4** (measured on fresh microcrystalline powders introduced in the magnetometer at low temperature to avoid solvent loss) are depicted in the figure 3 (χ_M being the molar magnetic susceptibility per Fe^{II} complex).

The $\chi_M T$ product of **4** is almost constant between 50 and 400 K and the measured value, 3.55 $cm^3\ mol^{-1}$ K, is coherent with that expected for a high-spin Fe^{II} complex (S = 2, g ≈ 2.18). In contrast, the $\chi_M T$ curves of **1-3** exhibit sigmoidal shapes that are typical of spin-crossover complexes. While weak $\chi_M T$ products measured at low temperature (*ca.* 0.15, 0.06 and 0.01 $cm^3\ mol^{-1}$ K for fresh samples of **1**, **2** and **3**, respectively) are in agreement with a Fe^{II} low-spin ions (S = 0), upon warming from 180 up to 400 K the $\chi_M T$ values increase gradually reaching *ca.* 3.11 (**1**), 3.40 (**2**) and 2.80 (**3**) $cm^3\ mol^{-1}$ K at 400 K. These values are lower than those expected for a Fe^{II} high-spin ions (with $\chi_M T$ ≈ 3.55 $cm^3\ mol^{-1}$ K and g ≈ 2.17) and inferior to the measured value in the analogue compound **4**. They point to incomplete spin crossover. The spin crossover observed upon cooling (and over several cycles) are identical for **1** and **2**. In contrast for compound **3**, the $\chi_M T$ product reverts to the diamagnetic state by following a different path upon cooling. This is associated to the loss of crystallization water molecules at high temperature as confirmed by thermogravimetric analysis (see ESI†). Indeed, a previously dehydrated sample **3d** exhibits the same $\chi_M T$ curve as that observed in the cooling mode after heating in the SQUID up to 400 K. Once dehydrated, the spin transition of **3d** is

reversible upon cycling. The transition temperature, $T_{1/2}$, of the spin transition for these compounds are *ca.* 316 (**1**), 277 (**2**), 342 (**3**, fresh) and 302 K (**3d**, dehydrated). The shift of 40 K observed between **3** and **3d** reveals the impact of the presence of solvate molecules in the crystal lattice on the SCO phenomenon in the solid-state.[22]

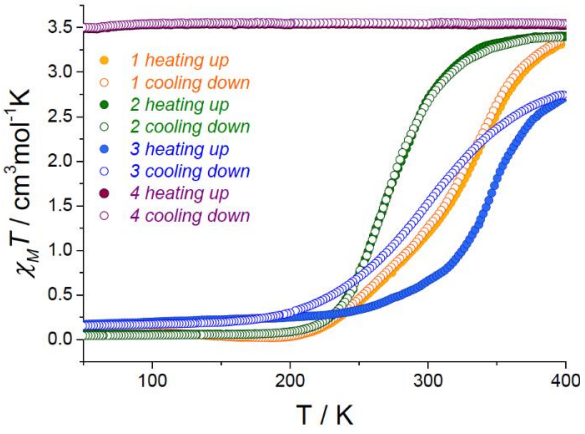

Figure 3. Solution and Solid-State Study of the Spin-Crossover $[Fe^{II}(R\text{-bik})_3](BF_4)_2$ complexes [R = Me, Et, Vinyl].

The solid-state $\chi_M T$ *vs* T data of **1-3** were fitted as commonly described in the literature by using the Slichter-Drickamer mean field model (equation 1),[23] in order to calculate the spin-equilibrium curves with an estimate of the associated thermodynamic parameters.

$$\ln\left[(1-n_{HS})/(n_{HS}-f_{HS})\right]=\left[\Delta H+\Gamma(f_{HS}+1-2n_{HS})\right]/RT \quad (1)$$

ΔH and ΔS are the enthalpy and the entropy variations at the experimental transition temperature ($T_{1/2}$) whereas the Γ parameter accounts for the co-operativity associated with the spin crossover (f_{HS} is the residual HS molar fraction at low temperature and n_{HS} represents the HS molar fraction).

Good fits were obtained for compound **2** (upon heating and upon cooling, respectively) and for dehydrated sample of **3d**, leading to the following values: ΔH = 29.3 and 29.6 (**2**), 32.9 (**3d**) kJ mol^{-1}; Γ = 0.78 and 0.45 (**2**), 1.0 (**3d**) kJ mol^{-1}, and $\Delta S = \Delta H / T_{1/2}$ = 107.2 and 107.4 (**2**), 100.0 (**3d**) J K^{-1} mol^{-1}; (see ESI†). The model partly fails in reproducing the experimental curve of **1** and **3** (fresh sample). This is not unusual for SCO systems and the search for more sophisticated models has been discussed earlier.[24,25] In the case of **1** and **3** the loss of solvent molecules during the experiment alters the shape of the spin transition and makes the simulation of the curves not so relevant (the transition temperatures are above room temperature and the experiments are carried out under reduced helium pressure). Overall, the Γ values are moderate and the $\Gamma/2RT_{1/2}$ ratio are well below the unit, as it is expected for gradual conversions. This is consistent with the weak intermolecular interaction that are observed in the crystal lattices of **1-3**. The estimated enthalpy (ΔH) and entropy (ΔS) values for **2-3d** are slightly above the usual range of the typical values observed for SCO compounds (ΔH = 3-27 kJ mol^{-1} and ΔS = 22-94 J K mol^{-1}).[26,27] However such high values of enthalpy and entropy variations have been already found in some cases of Fe^{II} SCO complexes.[7b, 28] Here the ΔS value is particularly high, well above the expected value due to the electronic entropy change (ΔS_{elec} = R ln 5 = 13.4 J K^{-1}). This points to the occurrence of important vibrational contributions, ΔS_{vib}. The ΔS_{vib} partly arises from the variation in the metal-ligand bond strength that accompanies the change in the metal-ligand bond distances upon the spin-state change. In the present case a noticeable contribution to ΔS_{vib} can also come from conformational changes occurring in the coordinated R-bik ligands (*e.g.* changes in the Fe-C-O angle and the planarity of the imidazolyl groups). As mentioned above, the □□diimine R-bik ligands are flexible, in contrast with □□diimine ligands such as 2,2'-bipyridine or 1,10-phenanthroline. Interestingly, we have recently shown that the planarity of the R-bik ligand can be notably affected in Fe-Co charge-transfer systems by the electronic-state of the coordinated metal.[29] Upon conversion of the high-spin Co^{II} into a low-spin Co^{III}, the ligand changes from a planar geometry (where the imidazolyl rings are located in the same plane) to a bent one, where the □-delocalization is lost. Such geometrical modifications alter not only the M-L vibration mode but also those of the ligands. The bending of the ligand will also affect its π-acceptor ability and contribute to significant change in the M-L bond strength and the enthalpy variation between the two spin-states. Unfortunately the loss of crystallinity of **1-3** at room temperature did not allow here to obtain the crystal structure of the high-spin state.

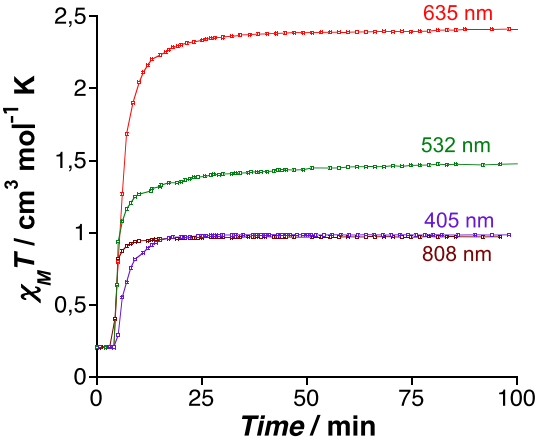

Figure 4. $\chi_M T$ *vs* irradiation time for **1** at 20 K under irradiation at 405, 532, 635; and 808 nm (*ca*. 5-10 mW/cm^2).

The Light-Induced Excited Spin State Trapping (LIESST) effect was investigated for the SCO complexes **1-3** (both fresh and dehydrated) by irradiating the samples at 20 K with laser diodes at 808, 635, 532, 405 nm (*ca*. 5-10 mW /cm^2). Compound **2** and **3d** do not show any photomagnetic effect in the present experimental conditions, whereas compounds **1** (Fig. 4) and **3** (see ESI†) exhibit respectively a moderate and a noticeable increase of the magnetization upon irradiation. The irradiation at 635 nm appears to be the most efficient in both cases. This wavelength is located near the maximum of an intense absorption band, which is observed in the solid-state UV-vis measurements (see ESI†). This band is ascribed to a MLCT band as confirmed by theoretical calculations (see ESI†). The irradiations at 532 nm (near the broad maximum of the MLCT band), at 808 nm (located in the tail of the MLCT band), and at 405 nm (located in a band ascribed to an Intra-ligand transition)

also show some efficiency. The $\chi_M T$ values reached after 50 min (of irradiation at 635 nm), 0.45 (**3**) and 2.39 (**1**) $cm^3\ mol^{-1}\ K$, are lower than expected for a HS Fe^{II} complex and they suggest a partial conversion of the diamagnetic state into a photo-induced paramagnetic state. The metastable states relaxes upon heating the sample (0.3 K / min) at T_{LIESST} = 57 (**3**) and 50 (**1**) K.

SOLUTION STUDIES

Magnetic susceptibility *versus* temperature measurements on solids are often used to determine relative amounts of HS and LS species. Their application on solutions, although possible, imply some experimental complications. As the spin equilibrium is often accompanied by changes in the optical properties, spin equilibrium can also be studied by measuring the temperature dependence of an absorption band, which is characteristic of one of the two spin states. For example, in Fe(II) complexes bearing π-acceptor ligands, the intensity of the MLCT band can be monitored to follow a spin-state change. However these experiments often require low-concentration solutions (*ca*. 10^{-4} M), which can lead to the dissociation of the complexes and erroneous data. In order to avoid this problem, it is better to use techniques that allow to work at higher concentrations. In the following section we compare different techniques including variable temperature (VT) ^{1}H NMR spectroscopy, Evans NMR method, solution state SQUID magnetometry in order to investigate the spin equilibria of **1-3** in acetonitrile solution.

^{1}H NMR solution study

The **basic concepts of paramagnetic NMR spectroscopy** were established several decades ago.[7,8] The main differences between the NMR of diamagnetic and paramagnetic species arise from the occurrence of an hyperfine interaction between the observed NMR nuclei and the unpaired electron(s). This interaction has two major impacts on the NMR spectrum: (1) it leads to strongly shifted signals, which can appear far outside of the normal range of diamagnetic molecules, making the structural analysis more difficult than for diamagnetic sample;[30] (2) the NMR signals can be significantly broadened (or even undetectable in some cases) due to fast nuclear relaxation. As the nuclear relaxation is inversely related to the electronic one,[31] the shorter the electronic relaxation times of the metal complex is, the sharper the NMR signals are. In some favourable cases, such as for Co^{II} octahedral paramagnetic complexes, spectra with good resolution can be obtained [32,33] so that it is possible to follow -as for diamagnetic species- chemical equilibrium by using VT NMR studies (*e.g.* substitution and isomerization processes).[32] Although the situation of HS Fe^{II} complexes is less favorable, some of these complexes can lead to well-resolved NMR features.[32,33] This is the case in our present study (see below).

In paramagnetic species, the chemical shifts bear structural information but also some magnetic information. Indeed, the observed chemical shift, δ_{obs}^T, can be expressed as a sum of a paramagnetic and a diamagnetic contribution:

$$\delta_{obs}^T = \delta_{dia} + \delta_{para}^T \quad (2)$$

The diamagnetic chemical shift contains the usual contributions to the chemical shift, which exist in diamagnetic molecules. It is generally estimated by measuring an isostructural diamagnetic reference. The paramagnetic chemical shift, δ_{para}^T, arises from the hyperfine interaction. δ_{para}^T , which depends on the temperature *T,* can be further decomposed as the sum of the pseudocontact term (δ_{PC}) and the Fermi-contact term (δ_{FC}):

$$\delta_{para}^T = \delta_{PC}^T + \delta_{FC}^T \quad (3)$$

The Fermi-contact term is a *through-bond* electron-nuclear interaction. It arises from the electron spin delocalization onto the observed nucleus (in other words, the spin density on the nucleus). As mentioned by McGarvey, the Fermi contact term can be expressed as a function of the magnetic susceptibility:[34]

$$\delta_{FC}^T = \frac{A^H}{3(\gamma_N/2\pi)\beta}\left(\frac{\chi_x}{g_x} + \frac{\chi_y}{g_y} + \frac{\chi_z}{g_z}\right) \quad (4a)$$

(where A^H is the hyperfine coupling constant, γ_N is the gyromagnetic ratio, χ_i and g_i are the component along the magnetic tensor axes). For a spin-only (S) isotropic system with no populated excited state, the formula is often simplified to:

$$\delta_{FC}^T = \frac{A^H g_{av}\beta}{3\gamma_N kT} S(S+1) \quad (4b)$$

(g_{av} is the average *g* value, *k* is the Boltzman constant). The contact chemical shift can thus be seen as a local paramagnetic susceptibility and its temperature dependence is proportional to 1/T, in agreement with the Curie law.

The pseudo-contact term, δ_{PC}^T , is a *through-space* electron-nuclear interaction and it comes from the dipolar coupling between the nuclear magnetic moment and the magnetic moment of the unpaired electron. This term strongly depends on the local magnetic anisotropy. For the simple case of an axial *g* tensor, it can be expressed through the simplified following equation:[8,34]

$$d_{PC} = \frac{m_0}{4p}\frac{bS(S+1)}{9kT}\frac{3\cos^2 q - 1}{r^3}(g_{//}^2 - g_\perp^2) \quad (5)$$

(β is the Bohr magneton, g_i are the component along the magnetic tensor axes, *r* is the distance between the magnetic source and the probed nucleus, θ is the angle between the main magnetic axis and the r direction). This term is small if the local magnetic anisotropy remains moderate. It also strongly depends on geometrical parameters. It can be negligible if the distance *r* is large, if the θ is close to 54° ($3\cos^2\theta$-1 ≈ 0).[35] However in some cases, when the anisotropy is not negligeable and the geometric parameter make the dipolar efficient, a deviation from the Curie law is observed. In these cases, the temperature dependence of the chemial shift can only be simulated by incuding additional terms (generally proportional to $1/T^2$).

In summary, if the dipolar contribution remains moderate for a given proton, the temperature dependence of the chemical shift will stricktly follow a Curie behavior. It is thus be possible to follow spin-crossover equilibria by studying the temperature dependence of selected chemical shifts.[6,36] In fact, as the Fe^{II} spin-state switching is faster than the NMR timescale, the observed proton NMR resonances represent the population-weighted average of the HS and LS states of the molecule at a given temperature. The peak shift is thus related to the amount of high-spin species:

$$\%_{HS} = \frac{(\delta_{obs}^T - \delta_{LS})}{(\delta_{HS} - \delta_{LS})} \times 100 \quad (6)$$

Here the δ_{LS} is the chemical shift observed for the pure diamagnetic Fe^{II} LS complex (S = 0) and it thus represent the δ_{dia} contribution. The accurate determination of the values for purely HS or LS species is not always accessible because of the limited temperature range (due to experimental limitation). In

such case the δ_{HS} or δ_{LS} values can still b□□estimat□□ by using □□□□□□□□□□□□□□□□

The NMR spectra of 1-3 (in CD_3CN at 310 K) together with the **peak assignments** are shown in Figure 5. These spectra are typical of paramagnetic species and contain (moderately) broad and strongly shifted temperature dependent signals.[37] In addition to the expected protons from the complexes (with up to five proton environments), each spectrum exhibit residual CHD_2CN, water and THF signals. In the case of **2**, small but noticeable signals due to the presence of free ligands are always observed. The signal assignment of the $[Fe^{II}(R\text{-}bik)_3](BF_4)_2$ complexes was done by using: (i) the relative integration of the signals; (ii) the comparison of the three derivatives (chemical substitution); (iii) the broadening of the signal. Indeed the major contribution to the nuclear relaxation arises from the dipolar contribution, which is proportional to $1/r^6$ (where r is the distance between the metal centre and the NMR nucleus).[8a] The protons close to the paramagnetic source can thus be identified as they show broader signal half-width.

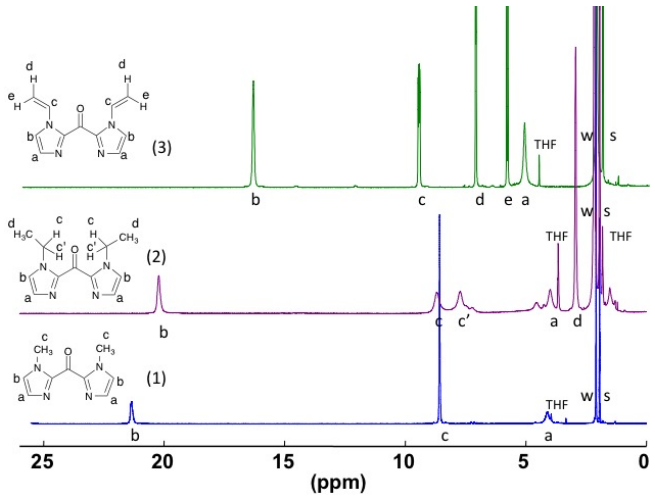

Figure 5. ^{1}H NMR specta of the $[Fe(Me\text{-}bik)_3](BF_4)_2$ **(1)**, $[Fe(Et\text{-}bik)_3](BF_4)_2$ **(2),** and $[Fe(V\text{-}bik)_3](BF_4)_2$ **(3)** complexes in CD_3CN at 310 K (w: water, s: solvent).

In **1**, the three signals of the Me-imidazole groups are observed with the relative intensity 1:1:3. At 310 K, the sharp signal at 8.57 ppm (c) with a relative intensity of 3H is unambiguously attributed to the CH_3 group of the ligand. The two signals with relative intensity 1H come from H^a and H^b. The broad signal near 4.10 ppm is assigned to H^a which is closer to the paramagnetic Fe^{II} centre. The other signal at 21.34 ppm is then attributed to the proton H^b.

In **2**, four different signals are observed for the Et-imidazole groups with the relative intensity 1:1:2:3**.** The sharp signal at 2.93 ppm (d) is assigned to the CH_3 group of the ligand. The broad signal near 3.99 ppm is assigned to H^a whereas H^b is observed at 20.22 ppm. At 310 K, the methylene protons of the ethyl group, (c) and (c'), are observed at 8.69 ppm and 7.73 ppm with the relative intensity 1:1. Indeed the Fe^{II} trischelate complex is chiral and these two protons are diastereotopic.[38a-b] It is also worth noticing that signals due to uncoordinated Et-bik ligand are always detectable in the NMR spectra of **2**.

In **3,** five signals of the vinyl-imidazole groups with the same intensity are observed at 310 K. The three vinylic protons are assigned according to their coupling constant value and considering that $J_{trans} > J_{cis} > J_{geminal}$ for the vinylic system. The two doublets at 7.20 ppm (d) and 5.89 ppm (e) are attributed to H^d and H^e respectively, whereas H^c appears as doublet of doublet (dd) near 9.55 ppm. The strongly shifted signal observed at 16.46 ppm is ascribed to H^b (as for **1** and **2**) and the broad H^a signal is observed at 5.17 ppm.

Table 3. Proton NMR data (δ in ppm) at 310 K in CD_3CN.

	H^a	H^b	H^c	$H^{c'}$	H^d	H^e
Me-bik	7.12	7.24	3.92			
Et-bik	7.40	7.04	4.51		1.45	
V-bik	7.22	7.68	5.07		7.57	5.51
(**1**) $[Fe(Me\text{-}bik)_3](BF_4)_2$	4.10	21.34	8.57			
(**2**) $[Fe(Et\text{-}bik)_3](BF_4)_2$	3.99	20.22	8.69	7.73	2.93	
(**3**) $[Fe(V\text{-}bik)_3](BF_4)_2$	5.17	16.46	9.55		7.20	5.89

The **variable temperature ^{1}H NMR studies** were carried out in the 230 - 350 K temperature range.[39] The spectra of **1**-**3** exhibit strong temperature dependence (Figures 6 and ESI†). While the ^{1}H chemical shifts are similar to those of the corresponding free ligands at 230 K, they strongly increase upon heating, spanning over 30 ppm at 350 K. This clearly accounts for a spin-state change from a diamagnetic LS state to a paramagnetic HS state upon heating. The increase of the signal half-width upon heating is also coherent with the occurrence of a paramagnetic state at high temperature. In contrast, the chemical shifts in compound **4** remain strongly shifted in all the probed temperature range but they tend to decrease significantly as the temperature increases (see ESI†), following the typical behaviour of paramagnetic species. More specifically, the observed $\delta \times T$ versus T curves vary linearly for all protons, showing that the high-spin model complex **4** follows a Curie law in the explored temperature range (see ESI).

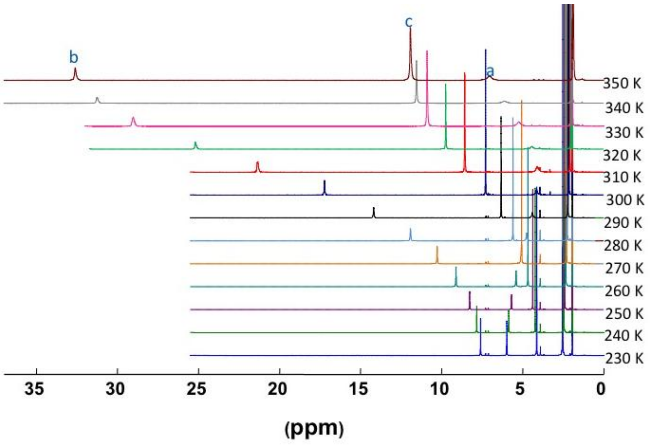

Figure 6. ^{1}H NMR spectra of $[Fe(Me\text{-}bik)_3](BF_4)_2$ (**1**) in CD_3CN in the 230-350 K temperature range.

The measured paramagnetic chemical shift, $\delta^T_{para} = \delta^T_{PC} + \delta^T_{FC}$, reflects the magnetic susceptibility of the complex (see equations 3-6). Therefore the temperature dependence of the paramagnetic signals can be conveniently used to follow the thermal population of the HS state (see above). Indeed, the plot of $\delta^T_{para}(H^b) \times T$ *versus* temperature for **1-3** show a sigmoidal shape, which is typical of spin-crossover complexes (Figure 7). Here we selected the H^b protons, which display sharp signal and exhibit the highest chemical shift variation with temperature to investigate the spin equilibria in **1-3** with more acuracy. It is also far enough from the paramagnetic center (above 5 Å) to lead to a reduced dipolar contribution (proportional to r^{-3}). All the other protons in these three complexes, except for H^a, exhibit the same trend and sigmoidal curves can be obtained similarly (see simulation in ESI). In the case of H^a, the chemical shift first slightly decreases then increases, as the temperature increases Here, the Fe^{II}-H^a distance is short, *ca*. 3 Å, this likely leads to a stronger pseudo-contact shift which may induce some deviation from the Curie law if the contact term is small.

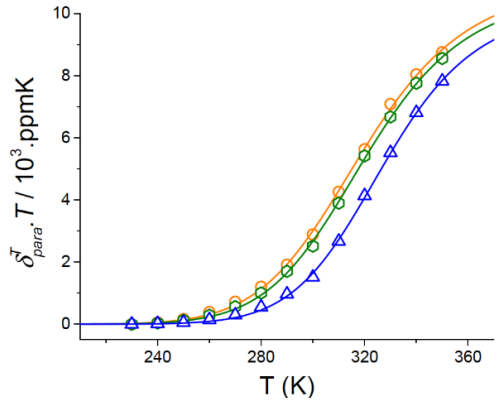

Figure 7. Thermal variation of the δ x *T* product for the H^b protons of three complexes (**1**, orange; **2**, green; **3**, blue respectively) obtained from variable temperature ^{1}H NMR study. The straight lines represent the simulated data (see text).

The comparison of the three curves shows that the change in the peripheral R group on the ligand has only a weak influence on the transition temperature. The temperature dependence of these chemical shifts can be modelled to extract the thermodynamic parameters of the Boltzmann spin equilibrium by using the following equation:[40]

$$\delta^T_{obs} \times T = \delta_{LS} \times T + \frac{C}{\left\{1+exp\left[\frac{\Delta H^\circ}{R}\left(\frac{1}{T}-\frac{1}{T1/2}\right)\right]\right\}} \quad (7)$$

where δ^T_{obs} is the experimental chemical shift and $\delta_{LS/dia}$ is the chemical shift in the diamagnetic state. The values extracted from these fits are given in the table 4. We assume that compounds **1-3** show a Curie like behaviour as observed in the high-spin Fe^{II} model compound **4** (see the magnetic and NMR data). The transition temperature obtained from the $\delta^T_{para}(H^b) \times T$ *versus T* plot are close to each other and in the 319-330 K temperature range. The thermodynamic values are of the same order as those found in the solid state and they compare to those obtained by other techniques below.

Interestingly, the variable temperature NMR study reveals also an unusual behaviour for the diastereotopic CH_2 protons in compound **2**: these protons are distinguishable in an intermediate temperature range, 270-310 K, but they overlap at T < 270 K and T > 310 K. In the low temperature range (230 - 260 K) the complex is diamagnetic. The chemical-shift range is moderate (0-12 ppm) and the separation between the signals is small so that only one peak is observed at 7.1 T. The use of higher magnetic field (*ca*. 14 T) is necessary to reveal the presence of the diastereotopic protons at low temperature (Figure 8).

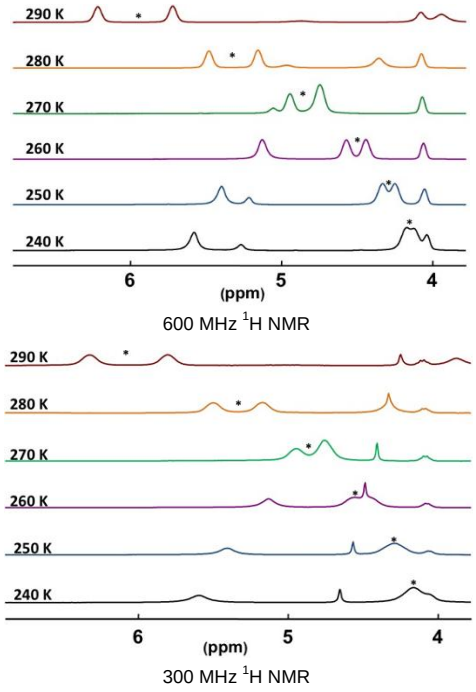

Figure 8. CH_2 diastereotopic signals (*) in **2** obtained from ^{1}H NMR at 300 MHz and 600 MHz.

Upon heating, the compound **2** becomes paramagnetic, the chemical-shift range is significantly broadened and the separation between the protons gradually increases from 230 K to 310 K. Although there is some signal broadening upon heating, the resolution is overall improved and the diastereotopic signal can be resolved. This effect is typical of paramagnetic species: the presence of small spin density delocalized on the probed nuclei allows a spreading of the NMR chemical shift range and leads to a "magnifying glass effect".[41] The resolution improves in many folds and it can be even better than that obtained by using external high magnetic field. Finally, at higher temperature (above 310 K) a coalescence occurs (see ESI†), indicating the occurrence of a rapid chemical exchange between the two diastereotopic protons. This is due to a rapid isomerization of the Δ and Λ enantiomers, relative to the NMR measuring time.

Magnetic susceptibility measurements through Evans NMR method and SQUID magnetometry.

The magnetic susceptibility was measured by Evans NMR methods and SQUID magnetometry on acetonitrile solutions of the paramagnetic complexes **1-3** (10^{-2} mol L^{-1}).[42] In the Evans experiments, the solutions were placed in an inner narrow-bore tube of a double-walled NMR tube. The difference between the solvent signal ($\Delta\upsilon$ in Hz) of a pure acetonitrile solution (outer

tube) and the solvent signal of the paramagnetic solutions (inner tube) is proportional to the bulk magnetic mass susceptibility:[43]

$$\chi = \frac{3\Delta\upsilon}{4\pi\upsilon m} + \chi_0 + \frac{\chi_0(d_0 - d_s)}{m} \qquad (8)$$

χ is the mass paramagnetic susceptibility, υ is the operating radio frequency of the spectrometer (3 x 10^8 Hz), m is the concentration of the paramagnetic ion in the inner tube in g cm^{-3}, χ_0 is the gram susceptibility of pure CD_3CN solvent (-0.534 X 10^{-6} g cm^{-3})[42], and d_0 and d_s are the density of the pure solvent and paramagnetic solution respectively.[44] For strongly paramagnetic substances, the last term is often neglected, so that the mass susceptibility becomes:

$$\chi = \frac{3\Delta f}{4\pi f m} + \chi_0 \qquad (9)$$

The molar susceptibility χ_M is calculated from χ in the usual way, and taking into account the diamagnetic contribution calculated from the Pascal tables.[45]

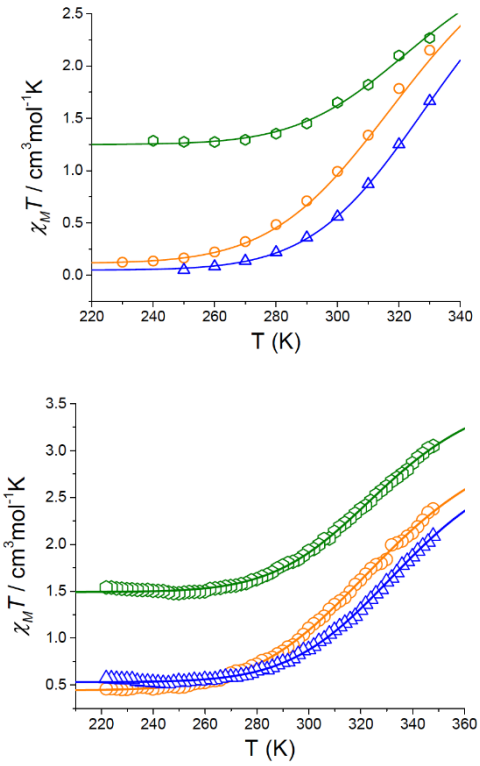

Figure 9. Thermal dependence of the $\chi_M T$ product for **1** (orange), **2** (green) and **3** (blue) obtained from susceptibility measurements in CD_3CN by using the Evans NMR method (up) and a SQUID magnetometer (down). The straight lines represent the simulated data (see text).

Because of solvent evaporation from the double-walled Evans tube, the explored temperature range was limited to 230 - 330 K. As shown in Figure 9, a gradual increase of the $\chi_M T$ product is observed upon heating, in agreement with the occurrence of a SCO process in solution. The transition starts at *ca.* 280 K and is incomplete at the highest available temperature. At 330 K, the measured $\chi_M T$ product of **1**, **2** and **3** are 2.15, 2.24 and 1.64 cm^3 mol^{-1} K, respectively. In contrast with the temperature-dependent ^{1}H NMR experiment described above, the limited temperature range does not allow an accurate determination of the values of the spin-equilibrium transition, $T_{1/2}$. In the case of **2**, the magnetic susceptibility of the solution is particularly high at low temperature and accounts for the presence of paramagnetic side product. This paramagnetic species has a fast relaxation as it is not detected by ^{1}H NMR (see above). As the only side product observed in the spectrum of **2** is the free Et-bik ligand, the paramagnetic side product is likely the high-spin $[Fe^{II}(Et\text{-}bik)_2(CH_3CN)_2](BF_4)_2$ complex, which is indeed NMR silent (*in situ* prepared complex does not exhibit any signals). A partial dissociation of the $[Fe^{II}(R\text{-}bik)_3](BF_4)_2$ complex would thus occur in the case of **2**.

The SQUID magnetometry measurements confirm the results obtained by Evans method (Figure 9). The $\chi_M T$ *vs* T curves measured on acetonitrile solution of **1**-**3** (in the temperature range 220-350 K and under a 1 T magnetic field) exhibit shapes similar to those found by using Evans and they are in agreement with the occurrence of spin-equilibria (starting from *ca.* 280 K and incomplete at 350 K). The $\chi_M T$ product for **1**, **2** and **3** measured at 330 K (2.00, 2.64 and 1.61 cm^3 mol^{-1} K respectively) compare quite well with those found by the Evans method at the same temperature. The presence of a paramagnetic species in the solution of **2** at low temperature is also confirmed by these measurements.

These magnetic data were fitted by using a simple solution model:[46,47]

$$ln\frac{1-n_{HS}}{n_{HS}} = \frac{\Delta H}{RT} - \frac{\Delta S}{R} \qquad (10)$$

The amount of HS complex, n_{HS}, or its relative fraction, γ_{HS}, is extracted from the equation:

$$\gamma_{HS}^{T} = \frac{(\chi_M T)_T - (\chi_M T)_{LT}}{(\chi_M T)_{HT} - (\chi_M T)_{LT}} \qquad (11)$$

$(c_M T)_T$ is the value of the product $(c_M T)$ at any temperature. The $(c_M T)_{LT}$ and $(c_M T)_{HT}$ correspond to the value of $c_M T$ at low temperature and high temperature respectively.

The thermodynamic parameters are finally obtained by fitting the equation:

$$(\chi_M T)_T = (\chi_M T)_{LT} + \frac{(\chi_M T)_{HT} - (\chi_M T)_{LT}}{1 + exp\left[\frac{\Delta H^\circ}{R}\left(\frac{1}{T} - \frac{1}{T_{1/2}}\right)\right]} \qquad (12)$$

The simulation of the curves lead to the similar values (table 4) and are in qualitative agreement with those found by other techniques (see comments below).

Table 4. Estimates of the thermodynamic parameters of the spin equilibria in **1**-**3** obtained from susceptibility measurements in solution using the regular solution model (*ca.* 10^{-2} mol/L).[36,46]

	VT ^{1}H NMR			Evans method			magnetometry		
	ΔH_{HL} [a]	ΔS_{HL} [b]	$T_{1/2}$ [c]	ΔH_{HL} [a]	ΔS_{HL} [b]	$T_{1/2}$ [c]	ΔH_{HL} [a]	ΔS_{HL} [b]	$T_{1/2}$ [c]
1	41	128	319	38	118	323	35	106	328
2	43	134	320	44	119	326	42	126	328
3	45	136	329	44	118	332	42	123	337

[a] in $kJmol^{-1}$, [b] in $Jmol^{-1}K^{-1}$ and [c] in K.

The results obtained from the method of Evans, the direct measurement of the magnetic susceptibility in solution, or the ^{1}H NMR study lead to coherent results. The transition temperatures, $T_{1/2}$, remain close to each other for the three techniques (319-

335 K). The values obtained for the vinyl-bik derivative, **3**, seem to be slightly higher (in all cases) than those measured for the **1** and **2**. Overall, the modification of the R group does not have a strong influence on the spin equilibrium in solution. This contrast with the situation in solid-state where small interactions (CH-π) seem to significantly affect the $T_{1/2}$ ($\Delta T_{1/2}$ = 65 K).

The thermodynamic parameters obtained for the three compounds are unusually high but they are coherent within the three techniques. They are also similar to the values obtained in the solid state where gradual transitions are observed. The VT NMR study (δT vs T measurement) appears to be more accurate over magnetometry techniques (SQUID magnetmetry or Evan's method) as small changes in the magnetic state of the probed complex can be reflected by important modifications in the chemical shifts. For instance, the chemical shift variation observed in ^{1}H NMR at variable temperature on the SCO complex are much more important than those observed on the solvent in the Evans method. Moreover the VT ^{1}H NMR allows the selective probing of the SCO complex. Indeed, the presence of paramagnetic impurities would bring more error sources in the magnetometry measurements. Here, the thermodynamic values deduced by probing directly an adequately chosen proton in **2** validate the estimated values obtained in magnetometry (where both compound **2** and a side product are measured).

Overall, the more pronounced sigmoidal curve is obtained from the variable temperature NMR study. The main advantage of this technique in comparison to the others is the following: the possible presence of other species does not interfere with the measurement, as the physical value measured is a selected chemical shift of the SCO complex, which directly reflects its magnetic state.

Computational Studies

To gain further insights into the electronic structure and magnetic properties of complexes **1**-**4**, we have undertaken density functional calculations using density functional theory (see experimental section). The spin state splitting of Fe(II) complexes which exhibit SCO properties are challenging for several exchange-correlation functional. Particularly functionals such as B3LYP*,[48] OPBE,[49] and B3LYP[50] has been recommended for the computation of spin state splitting. Due to considerably greater HF exchange (20% in B3LYP), hybrid functional such as B3LYP tends to weaken the M–L bonds, which stabilize the HS state compare to the LS state. On the other hand, dispersion and solvent effects shorten the M–L bonds which increase the bond dissociation energies and therefore favour the LS state. Here we have optimized the complexes **1**-**4** using B3LYP* and OPBE functionals with the incorporation of dispersion correction recommended by Grimme[51] and solvent effects as suggested earlier.[52] The computed energies using these functional suggest LS state as the ground state for B3LYP* and OPBE functionals; the estimated HS-LS gaps are 31.0, 37.2, 33.2 and 5.99 kJ mol^{-1} for complexes **1**-**4** using OPBE functional whereas B3LYP* functional yields 98.3, 73.4, 102.0 and 82.7 kJ mol^{-1} for complexes **1**-**4**. The single point energies computed using B3LYP on the other hand reveal high-spin as the ground state for all the complexes, the energy difference between the HS and LS states being 8.8, 6.0 and 6.1 kJ mol^{-1} for complexes **1**-**3**, respectively. For complex **4** on the other hand, calculations reveal a HS-LS gap of 20.7 kJ mol^{-1}, more than twice the value observed for other complexes. Although B3LYP*, OPBE clearly suggest LS ground state for **1**-**3**, the ground state predicted for complex **4** is contrary to experiments. However the energy difference obtained from OPBE and B3LYP* are very large and suggest in fact that SCO feature is not possible. The energies computed using B3LYP on the other hand are small and clearly suggest SCO features and therefore here we have elaborated the discussion on the structure and bonding using this functional. Besides theoretical studies on a series of {Fe^{II}N6} SCO complexes by various functionals suggests that although B3LYP fails to predict correct spin ground state multiplicity, the overall order of the HS-LS energy difference for a group of structurally related compounds are better described. For these reason, here we intend to employ B3LYP computed data for further discussion.[50]

The computed geometry for **1**-**4** at LS and HS states are given in Figure 10 and the structural parameters are summarized in Table 5 for all three functionals. Here we discuss in detail the geometry computed using B3LYP. Calculations clearly reveal that in all four cases the Fe-N distances in LS states are in the range of 2.03 to 2.05 Å while at the HS surface the bond lengths are in the range of 2.22 to 2.25 Å. The structural distortion is also quite significant in the high-spin geometry. The complex **4** exhibits the longest average Fe-N bond lengths and the maximum octahedral distortions among all the four computed complexes, in agreement with the X-ray structure and CShM analysis (see above). The distortions within the ligand geometry and twist in the planarity of the imidazole rings are reflected also in the optimized structures. The nature of the spin ground state is determined by the orbital splitting and the spin pairing energy. For complexes **1**-**4**, calculations yield the following electronic configuration $(d_{xz})^2(d_{yz})^1(d_{xy})^1(d_{x2-y2})^1(d_{z2})^1$ for the high-spin configuration.

To gain further insights into the nature of the bonding, we have plotted the d-based orbitals of complexes **1** and **4** (Figure 11). The presence of the ketone group in **1-3** promotes delocalization of the π clouds between the two imidazole rings leading to a stronger donor ability and thus a stabilization of the LS state. This feature is absent in complex **4** as depicted in Figure 11. The orbital splitting $\Delta E(d_{xz}\text{-}d_{z2})$ is estimated to be 1.476 eV, 1.450 eV and 2.438 eV for complexes **1**-**3** respectively. The close splitting pattern observed for complexes **1** and **2** is consistent with the similar $T_{1/2}$ values measured in solutions, while the relatively larger splitting pattern computed for complexes **3** is in agreement with a better stabilization of the LS state until *ca*. 335 K (see above). The participation of vinyl π orbital leads to a stronger interaction of the ligands with the d_{xz}/d_{yz} orbitals and to a larger orbital splitting and stabilization of the LS state (see ESI for Eigen-value plot of complexes **1**, **2** and **4**). This nicely correlates with the experimental results, as **3** exhibits a higher $T_{1/2}$ than **1** and **2**.

Besides, significant C-H$^{\cdots}$O interactions are detected between the alkyl/vinyl hydrogen and the ketone oxygen atoms in complexes **1**-**3**.[53] The strength of this interaction varies within the set of complexes **1**-**3**, in line with the C-H$^{\cdots}$O distances, which are 2.55, 2.30 and 2.26 Å for complexes **1**, **2** and **3**, respectively. This interaction is found to weaken the donor abilities of the imidazole ring. However its effect remains small

and does not compensate the dominant π-acceptor contribution that lead to a stronger ligand field in the vinyl complex.

Table 5. B3LYP OPBE and B3LYP* optimized selected bond and angle parameters for complex **1**-**4**.

B3LYP

Bonds and angles	Complex **1**		Complex **2**		Complex **3**		Complex **4**	
	HS	LS	HS	LS	HS	LS	HS	LS
Fe-N1	2.226	2.043	2.229	2.034	2.233	2.040	2.248	2.055
Fe-N2	2.237	2.043	2.231	2.042	2.224	2.038	2.235	2.046
Fe-N3	2.234	2.044	2.227	2.043	2.232	2.037	2.232	2.040
Fe-N4	2.237	2.043	2.239	2.042	2.233	2.039	2.245	2.055
Fe-N5	2.227	2.044	2.224	2.034	2.232	2.044	2.226	2.061
Fe-N6	2.234	2.043	2.229	2.043	2.224	2.031	2.232	2.046
N3-Fe-N6	174.4	178.6	173.8	178.8	174.4	179.5	172.1	178.2
ρ(Fe)[a]	3.88	0.00	3.83	0.00	3.87	0.00	3.89	0.00

OPBE

Bonds and angles	Complex **1**		Complex **2**		Complex **3**		Complex **4**				
	HS	LS	HS	LS	HS	LS	HS	LS			
Fe-N1	2.130	1.942	2.113	1.919	2.136	1.929	2.150	1.938			
Fe-N2	2.128	1.923	2.132	1.932	2.121	1.918	2.158	1.931			
Fe-N3	2.132		1.935		2.122		1.947	2.131	1.941	2.176	1.958
Fe-N4	2.128		1.935		2.122		1.947	2.135	1.944	2.157	1.958
Fe-N5	2.124		1.923		2.133		1.938	2.113	1.925	2.144	1.931
Fe-N6	2.132		1.942		2.113		1.919	2.132	1.935	2.155	1.938
N3-Fe-N6	177.6		179.7		178.9		174.9	176.6	179.5	177.4	179.9
ρ(Fe)[a]	3.91		0.00		3.91		0.00	3.92	0.00	3.78	0.00

B3LYP*

Bonds and angles	Complex **1**		Complex **2**		Complex **3**		Complex **4**	
	HS	LS	HS	LS	HS	LS	HS	LS
Fe-N1	2.147	1.978	2.155	1.963	2.147	1.974	2.168	1.990
Fe-N2	2.136	1.965	2.133	1.976	2.130	1.958	2.149	1.976
Fe-N3	2.138	1.980	2.129	1.984	2.139	1.976	2.146	1.996
Fe-N4	2.149	1.980	2.126	1.984	2.136	1.977	2.147	1.990
Fe-N5	2.139	1.965	2.126	1.976	2.126	1.962	2.150	1.970
Fe-N6	2.141	1.978	2.162	1.963	2.145	1.978	2.187	1.984
N3-Fe-N6	176.7	179.7	169.9	176.0	175.2	179.4	169.9	179.1
ρ(Fe)[a]	3.78	0.00	3.79	0.00	3.79	0.00	3.68	0.00

[a] spin density on the Fe

This is also supported by the computed spin densities where complexes **1**-**3** possess a net spin density of 3.888 at the Fe atom for the HS spin state while complex **4** has slightly higher spin density at the Fe atom (3.890). Computed spin density plots of complexes **1** and **4** are shown in Figure 12. The spin density at the metal centre has an octahedral shape and is partially delocalized onto the ligands. The nitrogen atom coordinated to the Fe centre in complex **1** has a spin density in the range of 0.021-0.023 while the corresponding atom in complex **4** spans in the range of 0.016 to 0.026. The oxygen atom of the ketone group also exhibits some spin densities in complexes **1**-**3**. Although the quoted values are small, the differences observed clearly indicates significant structural and electronic alteration upon ligand modifications leading to variations in the SCO properties.

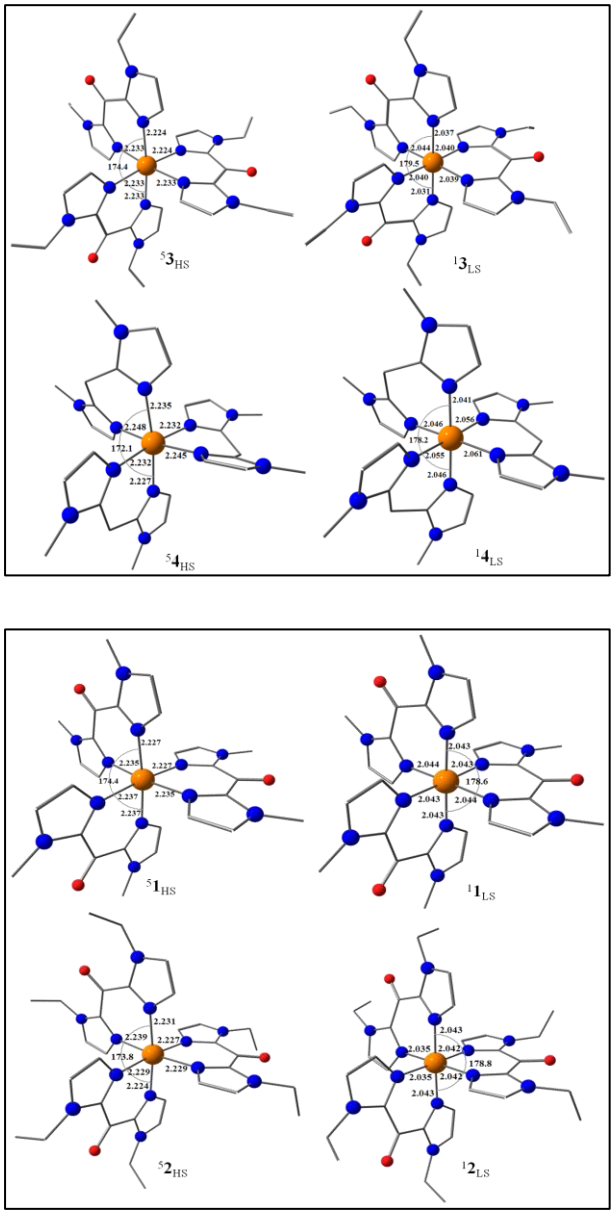

Figure 10. B3LYP computed optimized HS and LS geometries for **1-4**. Colour code Blue=N; Red =O; Grey=Carbon. Hydrogen atoms are omitted for clarity.

In order to evaluate the parameters that are correlated to the spin-crossover properties, we have estimated ΔS and $T_{1/2}$ values for complexes **1**-**3**. The $T_{1/2}$ can be computed from the electronic energy, vibrational and entropic contributions to the energy using the following equation as advocated earlier.[54]

$$T_{1/2} = \left[\Delta E_{el}(0) + \Delta E_{vib}\left(T_{\frac{1}{2}}\right)\right] / \Delta S\left(T_{\frac{1}{2}}\right) \quad (13)$$

Here where $\Delta E_{el}(0)$ is the electronic energy difference between the high-spin and low-spin state along with the zero point energy correction and the thermal correction to electronic energy. ΔE_{vib} is the vibration due to thermal energy and ΔS is the entropy of the system.

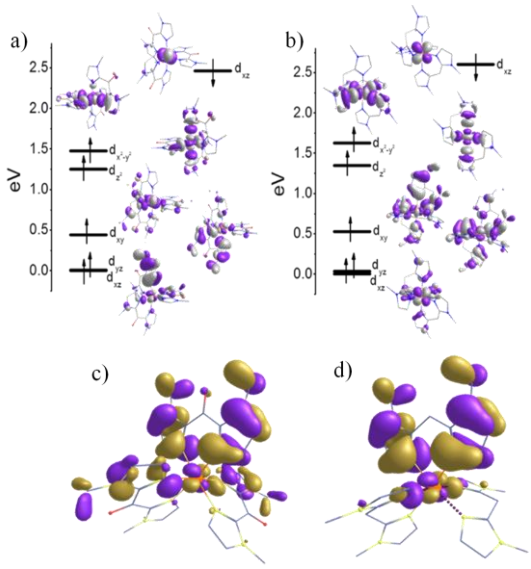

Figure 11. Energy splitting of d-based orbital's for (a) complex **1** and (b) complex **4**; Molecular orbital (MO) diagram showing the presence of a more extended π-interaction in complex **1** (c) than in complex **4** (d).

Table 6. Estimates of the thermodynamic parameters of the spin equilibria estimated using DFT calculations for complexes **1**-**3**.

Compounds	ΔH_{SCO} (KJ mol^{-1})	ΔS_{SCO} (J mol^{-1} K^{-1})	$T_{1/2}$ (K)
[Fe(Me-bik)$_3$] (BF$_4$)$_2$	25.6	59.6	308.5
[Fe(Et-bik)$_3$] (BF$_4$)$_2$	22.8	53.4	277.1
[Fe(V-bik)$_3$] (BF$_4$)$_2$	25.6	36.7	438.5

The vibrational and entropic contributions are estimated from frequency calculations as discussed in the experimental section. The ΔS values are estimated to be 59.6, 53.4 and 36.7 J K^{-1} mol^{-1} for complexes **1**-**3** respectively (see table 6). These values are small as compared with the experimental ones but they do not take into account a possible conformational change in the ligand upon spin-state change as discussed above. On the other hand the ΔE_{vib} are estimated to be −0.8, −1.4, and −2.2 K cal. mol^{-1}. The estimated $T_{1/2}$ values, 308.5, 277.1 and 438.5 complexes **1**-**3** are different compared to the experimental *ones*, but the largest value computed for complex **3** is consistent with the observed trend in the experiments.

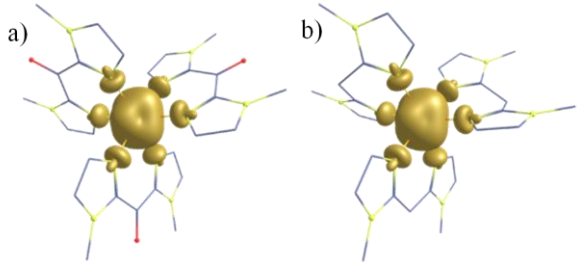

Figure 12. B3LYP computed spin densities for complex **1** (a) and complex **4** (b) in high-spin state.

Conclusions

In this work, we have studied in both solid state and solution the SCO phenomenon of closely related [Fe^{II}(*R*-*bik*)$_3$]$^{2+}$ complexes containing similar β-diimine ligands. Our goal was to evaluate the influence of the ligand functionalization over the switching properties of these systems. DFT calculations were also compared to experimental results aiming at rationalizing the magnetic properties.

The theoretical calculations based on density functional methods have been performed for all four complexes and the employed methodology gave a satisfying description of both the structure and electronic properties of these complexes. The computed energy difference between the HS and LS structures rationalize the presence of SCO properties in complexes **1**-**3.** The theoretical calculations permit to clarify the critical role of the central ketone group on the magnetic and optical properties of the studied complexes. The computed electronic structures and spin densities revealed that the C=O group in complexes **1**-**3** favor a □ delocalization between the two imidazole rings. This leads to an enhancement of the ligand π-acid character, and therefore an increase of the ligand field strength leading to the stabilization of LS state as the ground state. Indeed, whereas the [Fe^{II}(bim)$_3$]$^{2+}$ model complex remains high spin, the derivative complexes containing the α–keto–β-diimine ligands exhibit a stronger ligand field and show SCO behaviour near room temperature.

The *R* groups in the *R*-*bik* ligands were shown to have a moderate influence on the $T_{1/2}$ measured in solution. Inductive attractive group (vinyl) were expected to reduce the ligand field and stabilize the high-spin state, *i.e*. leading to a decrease of the $T_{1/2}$. Conversely inductive donor groups (ethyl and methyl) were expected to lead to an increase of the $T_{1/2}$. The observed trend is opposite and tends to show that the vinyl group contribute to the delocalization of the □-system, leading to a higher □-acid character and a stronger ligand field. The DFT computed MO diagram enlightens this point as stronger interaction of the ligands with d_{xz}/d_{yz} orbitals are detected. The differences remain however moderate with $T_{1/2}$ increasing by 10-15 K from the donor alkyl to the attractive vinyl group. The weak C-H$^{\cdots}$O between the alkyl/vinyl and ketone groups may also influence the ligand field induced by these ligands. The interaction is found to be stronger in the case of the vinyl-bik ligand but its effect remains apparently moderate.

To analyse the spin-crossover process in solution, we used three different methods including the Evans NMR method. This technique gives access to the bulk susceptibility of the solution, so if paramagnetic side-product(s) are present in solution (or if chemical exchange occurs) the measurement can lead to ambiguous results, as illustrated in compound **2**. Bulk susceptibility was also extracted from measurement in solution by using SQUID magnetometry. Although the SQUID technique is more sensitive than the Evans method (more diluted solutions can be studied), it suffers from similar inconveniences. Overall, in the present experimental conditions, the best SCO equilibrium curves (with the more pronounced sigmoidal shape) are obtained from the NMR study. By tracking the temperature dependence of adequately chosen ^{1}H chemical shift (which bears a strong contribution from the Fermi contact term), we were able to follow the spin-crossover process of the three

compounds. In this case, the possible presence of other paramagnetic species does not interfere with the measurements since the physical value measured is a selected chemical shift of the SCO complex, which directly reflects its magnetic state. The thermodynamic values ΔH and ΔS deduced from these measurements are high but coherent within the three techniques, and in the same order of magnitude for the three complexes. The high ΔS value is probably related to the change in the ligand conformation between the HS and LS state. Although it was not possible to obtain a crystal structure of the HS state (because of the loss of crystallinity), such changes in the ligand geometry were previously observed in other switchable molecule containing the R-bik ligand.[28]

Beside the study of the spin equilibrium, ^{1}H NMR allowed us to study the stability of the species over the explored temperature range and the possible occurrence of chemical equilibrium, provided that the paramagnetic species have suitable NMR signals (*i.e*. convenient nuclear relaxation time). Interestingly, we were able to observe in the case of compound **2** an isomerization between the two Δ-Λ stereoisomers. Whereas the two isomers cannot be detected at low temperature (since the signals are diamagnetic) unless high-field NMR spectroscopy is used, at higher temperature, the presence of spin density on the probed nuclei led to an enlargement of the chemical shift range and an improved resolution (as long as coalescence does not occurs).

Finally, variable temperature susceptibility data were used to analyse the spin-transition process in solid state and to extract the associated thermodynamic parameters. The spin transition temperatures, which are close to each other in solution, are clearly spread in a broader temperature range in the solid-state. They are respectively close to (316 K in **1**), higher (342 K in **3**) and lower (277 K in **2**) than those measured in acetonitrile solution. The intermolecular interactions and the solid-state organization clearly affect the energetic of the system. Overall the spin-transition remain gradual, with almost no cooperative effect as only weak intramolecular interactions are observed in the structures of compounds **1-3**. In contrast with **1** and **2**, the transition observed for compound **3** is clearly affected by the loss of solvent molecules occurring upon heating.

Experimental Section

Materials. All chemicals and solvents were purchased from Sigma Aldrich and Alfa Aesar and used as received. All the experiments were carried out under aerobic conditions (except for the synthesis of compound **4**).

Instrumentation. FTIR spectra were recorded over the range of 4000-400 cm^{-1}. Measurements were carried out on a Tensor 27 Bruker instrument working in the ATR mode (on fresh samples). Solid-state UV-vis spectra were measured at room temperature on a PerkinElmer Lambda 1050 WB spectrophotometer. The measurements were performed on KBr pellets. Thermogravimetric analysis were carried out with a TGA analyzer (TAI instrument, SDT Q600) at a rate of 2 °C min^{-1} under N_2 flow (100 mL/min). **Magnetic studies.** Magnetic susceptibility data were collected using a Quantum Design SQUID magnetometer (MPMS-5S) calibrated against a standard palladium sample. The magnetic susceptibility values were corrected from the diamagnetism of the molecular constituents using Pascal's table[45] and from the sample holder. The measurements in the solid state were carried out on polycrystalline samples of **1**-**4** in the temperature range 4-400 K in a 1 T magnetic field. The susceptibility measurements of solutions of **1-3** (10^{-2} mol L^{-1}) were carried out in the temperature range 220-350 K under an external magnetic field of 1 T. The rapid evaporation of CH_3CN above 350 K and its freezing below 220 K prevent us from exploring a broader temperature range. Diamagnetic corrections were estimated by measuring the same amount of pure CH_3CN solution in the same container. Photomagnetic measurements on fresh samples of **1-3** were carried out by using a sample holder equipped with an optical fibre. In a typical experiment 0.4 mg of ground crystals were deposited on an adhesive tape. The sample was separated from the end of the fibre by *ca*. 5.5 cm. All the irradiations were carried out at 20 K to minimize the temperature variation induced by the LASER light.

NMR spectroscopic studies. The NMR spectra of 1-3 were recorded on a Bruker Avance^{II} 300 spectrometer operating at a ^{1}H Larmor frequency of 299.95 MHz and equipped with a BBMS variable-temperature unit. A variable temperature NMR experiment was also carried out for 2 on a Bruker Avance^{II} 600 spectrometer (^{1}H Larmor frequency of 600.13 MHz). The concentration of all three paramagnetic samples was 10^{-2} mol L^1 for all the experiments. The spectra were collected over the 230 - 350 K temperature range (for variable temperature ^{1}H NMR) and 230 - 330 K (for Evans' NMR). The observed signals are referenced using the solvent proton signal (1.94 ppm relative to TMS). The temperature was calibrated using the standard Wilmad methanol and ethylene glycol samples for low and high temperatures respectively.

Ligand synthesis. Ligands including Me-bik [bis(1-methylimidazol-2-yl)ketone], Et-bik [bis(1-ethylimidazol-2-yl)ketone], V-bik [bis(1-vinylimidazol-2-yl)ketone], bim [bis(1-methylimidazol-2-yl)ketone] were prepared according to literature procedures.[51,52]

Synthesis of compounds 1-4.

$[Fe(Me\text{-}bik)_3](BF_4)_2\cdot 0.25\ H_2O$ (1) and $[Fe(Et\text{-}bik)_3](BF_4)_2$ (2) Similar synthetic procedures were applied for 1 and 2. To a methanolic (20 mL) solution of the ligand (Me-bik: 285 mg; Et-bik: 327 mg; 1.5 mmol) was added a colourless solution of $Fe(BF_4)_2\cdot 6H_2O$ (169 mg, 0.5 mmol) in methanol (5 mL), The resulting deep blue solution was stirred for 30 minutes at room temperature and filtered. $[Fe(Me\text{-}bik)_3](BF_4)_2\cdot 0.25\ H_2O$ and $[Fe(Et\text{-}bik)_3](BF_4)_2$ were obtained as dark plate-like crystals after a few days by slow evaporation of the solution under ambient conditions. Yield: 77 % (1), 55 % (2).

1: ^{1}H NMR (300 MHz, CD_3CN), 300 K: δ (ppm) = 4.14 (s, 2H, H_{im}), 7.29 (s, 6H, CH_3), 17.22 (s, 2H, H_{im}). ATR-IR (solid): ν (cm^{-1}) = 3139.9, 2980.0, 1636.6, 1523.2, 1486.1, 1413.0, 1291.2, 1166.0, 1035.1, 896.9, 785.0, 769.3 cm^{-1}. Anal. Calcd for $C_{27}H_{30.5}B_2F_8FeN_{12}O_{3.25}$: C, 40.31; H, 3.82; N, 20.89 Found: C, 40.71; H, 3.89; N, 20.78. ESI-MS: *m/z* 313.30 $\{[Fe^{II}(Me\text{-}bik)_3]^{2+}$, calcd 313.10}, 523.30 $\{[Fe^{II}(Me\text{-}bik)_2(BF_4)]^+$, calcd 523.10}, 713.60 $\{[Fe^{II}(Me\text{-}bik)_3(BF_4)]^+$, calcd 713.40}.

2: ^{1}H NMR (300 MHz, CD_3CN), 300 K: δ (ppm) = 4.12 (s, 2H, H_{im}), 2.47 (s, broad, 6H, CH_3), 16.02 (s, 2H, H_{im}), 7.39 (s, broad, 2H, CH_2), 6.72 (s, broad, 2H, CH_2). ATR-IR (solid): ν (cm^{-1}) = 3125.6, 2987.7, 1637.4, 1475.6, 1405.5, 1292.9, 1162.9, 1028.0, 890.8, 790.5, 769.6 cm^{-1}. Anal. Calcd for $C_{33}H_{42}B_2F_8FeN_{12}O_3$: C, 44.83; H, 4.79; N, 19.01 Found: C, 45.33; H, 4.88; N, 19.10. ESI-MS: *m/z* 219.30 $\{[(Et\text{-}bik)+H]^+$, calcd 219.21}, 241.16 $\{[(Et\text{-}bik)+Na]^+$, calcd 241.11}, 355.21 $\{[Fe^{II}(Et\text{-}bik)_3]^{2+}$, calcd 355.13}, 443.27$\{[Fe^{II}(Et\text{-}bik)_3(BF_4)_2+2H]^{2+}$, calcd 443.16}, 459.28 $\{[(Et\text{-}bik)_2+Na]^+$, calcd 459.40}.

$[Fe(V\text{-}bik)_3](BF_4)_2\cdot 1.5\ H_2O$ (3). To a solution of V-bik (321 mg, 1.5 mmol) in a (4/1) mixture of acetonitrile / water (20 mL) was added a colourless solution of $Fe(BF_4)_2\cdot 6H_2O$ (169 mg, 0.5 mmol) in the same solvent (5 mL). The resulting blue solution was then stirred for 30 minutes at room temperature and filtered. $[Fe(V\text{-}bik)_3](BF_4)_2$ was obtained as dark plate like crystals after two weeks by slow evaporation of the solution under ambient conditions. Yield: 75%.

3: ^{1}H NMR (300 MHz, CD_3CN), 300 K: δ (ppm) = 5.37 (s, 2H, H_{im}), 6.45 (d, 2H, CH_{vinyl}), 12.88 (s, 2H, H_{im}), 8.92 (dd, 2H, CH_{2vinyl}), 5.78 (d, 2H, CH_{2vinyl}). ATR-IR (solid): ν (cm^{-1}) = 3139.4, 2982.0, 1643.1, 1472.9, 1425.7, 1315.6, 1278.0, 1157.6, 1033.7, 955.6, 891.4, 790.9, 765.6 cm^{-1}. Anal. Calcd for $C_{33}H_{32}B_2F_8FeN_{12}O_{4.5}$: C, 44.08; H, 3.70; N, 18.69 Found: C, 44.15; H, 3.68; N, 18.70. ESI-MS: *m/z* 242.05 $\{[Fe^{II}(V\text{-}bik)_2]^{2+}$, calcd 242.05}, 349.09 $\{[Fe^{II}(V\text{-}bik)_3]^{2+}$ calcd 349.10}, 451.16 $\{[(V\text{-}bik)_2+Na]^+$,

calcd 451.17}, 503.10 {[Fe^{II}(V-bik)$_3$(BF_4)$_3$+2Na+H]$^{2+}$, calcd 503.09}, 571.11 {[Fe^{II}(V-bik)$_2$(BF_4)]$^+$, calcd 571.11}, 621.15 {[Fe^{II}(V-bik)$_2$(BF_4)(H_2O)(MeOH)] $^+$, calcd 621.15}, 785.20 {[Fe^{II}(V-bik)$_3$(BF_4)]$^+$, calcd 785.23}.

[Fe(bim)$_3$](OTf)$_2$ (4). A solution of $Fe^{II}(OTf)_2$·2MeCN (124 mg, 0.28 mmol) in dry THF (5 mL) was added dropwise to a stirred solution of bim ligand (150 mg, 0.85 mmol) in dry THF (10 mL) under inert atmosphere. The resulting suspension was stirred at room temperature overnight. The white solid was then filtered and washed twice with 10 mL of THF. Layering of toluene with an acetonitrile solution of 4 gave colourless needle-like crystals within 2 days. Yield: 75%. The compound has to be stored in an oxygen-free medium to avoid the oxidation of the ligand that leads to the formation of the [Fe(Me-bik)$_3$]$^{2+}$ complex.

4: ^{1}H NMR (400 MHz, CD_3CN), 300 K: δ (ppm) = 0.87 (s, 2 H, CH_2), 12.63 (s, 6H, CH_3), 39.70 (s, 2H, H_{im}), 43.69 (s, 2H, H_{im}). ATR-IR (solid): ν (cm^{-1}) = 3134.6, 2959.0, 1541.2, 1508.0, 1412.3, 1327.5, 1262.1, 1148.1, 1124.0, 1031.4, 955.9, 754.1, 747.2 cm^{-1}. Anal. Calcd for $C_{29}H_{36}F_6FeN_{12}O_6$: C, 39.46; H, 4.11; N, 19.04; S, 7.13 Found: C, 39.37; H, 4.21; N, 18.64; S, 7.13.

X-ray crystallography. A single crystal of each compound was selected, mounted and transferred into a cold nitrogen gas stream. Intensity data was collected with Bruker Kappa-APEX2 systems using micro-source Cu-Kα (1,3,4) or fine-focus sealed tube Mo-Kα (2) radiations. Unit-cell parameters determination, data collection strategy, integration and absorption correction were carried out with the Bruker APEX2 suite of programs. The structures were solved using SIR92[53] (1,2), SHELXS-86[50] (3) or Superflip[54] (4) and refined anisotropically by full-matrix least-squares methods using SHELXL2014[55] within the WinGX[55] suite (1,2) or CRYSTALS[56] (3,4). The structures were deposited at the Cambridge Crystallographic Data Centre with numbers CCDC 1481941-1481944 and can be obtained free of charge via www.ccdc.cam.ac.uk. Crystallographic details are given in Table S1.

Computational studies. DFT[57] calculations were performed on the X-**ray** structural coordinates using the Gaussian 09[58] and ORCA[59] 2.9.1 suite programs for all the four complexes. Calculations were performed in two steps i) optimizing the nuclear coordinates of the X-ray structure and ii) on top of the optimized coordinates frequency calculations were performed to extract the thermodynamic parameters. All calculations employ Becke's exchange functional [60] together with correlation functional of Lee, Yang and Parr[61] (B3LYP as implemented in Gaussian) along with Ahlrichs polarised triple-ζ valence (TZVP)[62] basis set for the metal ion and Pople's split valence polarised 6-31G** [63] basis set for rest of the atoms. The frequency calculations were performed using OPBE[64] functional as this has been shown to be superior in estimating thermodynamic quantities.[65]

Keywords: Spin Crossover • iron(II) • β-diimine ligand • paramagnetic NMR • DFT calculations

Entry for the Table of Contents (Please choose one layout)

Layout 1:

FULL PAPER

A series of Fe^{II} spin-crossover (SCO) complexes containing of β-diimine ligands were synthesized and characterized. The foregoing results particularly demonstrate the efficiency of variable temperature ^{1}H NMR chemical shift as a useful alternative for studying spin-crossover equilibrium in solution.

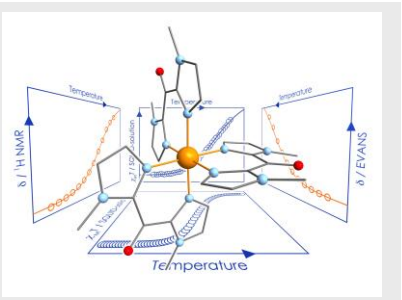

Spin-crossover complexes

S. De, S. Tewary, D. Garnier, Y. Li, G. Gontard, L. Lisnard, A. Flambard, F.Breher,M. L. Boillot, G. Rajaraman,* and R. Lescouëzec*

Page No. – Page No.

Solution and Solid-State Study of the Spin-Crossover $[Fe^{II}(R\text{-}bik)_3](BF_4)_2$ complexes [R = Me, Et, Vinyl]

[1] a) F.-B. Lopez, R. Byrne, Y. Wu, L. Nolan; J. Kim, K.-T. Lau, G.-G. Wallace, D. Diamond, *ECS Trans.* **2009***, 19,* 199-210*;* b) S. Cobo, G. Molnár, J.-A. Real, A. Bousseksou, *Angew. Chem. Int. Ed.* **2006***, 45,* 5786-5789.
[2] a) C.-J. Fang, Z. Zhu, W. Sun, C.-H. Xu, C.-H. Yan, *New J. Chem*. **2007***, 31,* 580-586*;* b) M.-D. Ward, *J. Chem. Educ.* **2001***, 78,* 321-328.
[3] a) O. Kahn, J.-P. Launay, *Chemtronics.* **1988***, 3,* 140; b) O. Kahn, C.-J. Martinez, *Science.* **1998***, 279,* 44-48.
[4] a) "Topics in Current Chemistry", *Spin Crossover in Transition Metal Compounds I.-III.* (Eds.: P. Gütlich, H.A. Goodwin), Springer-Verlag, Berlin/Heidelberg, Germany. **2004**, vol. 233−235*;* b) J.-A. Real, A.-B. Gasper, M.-C. Muñoz, *Dalton Trans*. **2005**, 2062-2079.
[5] A. Bousseksou*,* G. Molnár*,* G. Matouzenko*, Eur*. *J. Inorg*. *Chem*. **2004**, 4353-4369*.*
[6] L.-A. Yatsunyk, F.-A. Walker, *Inorg. Chem.* **2004**, *43*, 757-777.
[7] a) G.-N. La Mar, F.-A. Walker in *The Porphyrins*, *Vol. IV* (Eds.: D. Dolphin) Academic Press: New York. **1979***,* 61*;* b) S.-E. Creutz, J.-C. Peters, *Inorg. Chem*. **2016**, *55*, 3894-3906; c) H. Peltzold, P. Djomgoue, G. Hörner, J. M. Speck, T. Rüffer, D. Schaarschmidt, *Dalton trans*. **2017**, 45, 13798-13809; d) R. G. Miller, S. Brooker, Inorg. Chem., **2015**, 54, 5398-5409.
[8] a) F.-H. Köhler in *Magnetism: Molecules to Materials. Models and Experiments*, *Vol. IV* (Eds.: J.-S. Miller, M. Drillon) Wiley-VCH: Weinheim, Germany. **2001***,* 379*;* b) F.-A. Walker in *The Porphyrin Handbook*, *Vol. 5* (Eds.: K.-M. Kadish, K.-M. Smith, R. Guilard) Academic Press: London, U.K. **2000***,* 81.
[9] See for example : S. Schlamp, K. Dankhoff, B. Weber, *New. J. Chem.* **2014**, 38, 1965
[10] a) J. Mercurol, Y. Li, E. Pardo, O. Risset, M. Seuleiman, H. Roussèliere, R. Lecouëzec, M. Julve, *Chem. Commun*. **2010**, *46*, 8995-8997; b) A. Mondal, Y. Li, M. Seuleiman, M. Julve, L. Toupet, M. Buron-Le-Cointe, R. Lescouëzec *J. Am*. *Chem*. *Soc*. **2013***, 135,* 1653-1656.
[11] a) A. Mondal, Y. Li, P. Herson, M. Seuleiman, M.-L. Boillot, E. Rivière, M. Julve, L. Rechignat, A. Bousseksou, R. Lescouëzec, *Chem*. *Commun*. **2012***, 48,* 5653-5655*;* b) A. Mondal, L.- M. Chamoreau, Y. Li, Y. Journaux, M. Seuleiman, R. Lescouëzec, *Chem.–Eur. J.* **2013***, 19,* 7682-7685*;* c) A. Mondal, Y. Li, L.-M. Chamoreau, M. Seuleiman, L. Rechignat, A. Bousseksou, M.-L. Boillot, R. Lescouëzec, *Chem*. *Commun*. **2014***, 50,* 2893-2895.
[12] a) C. Graaf, C. Sousa, *Chem.–Eur. J.* **2010***, 16,* 4550-4556; b)*,* W. Gawelda, A. Cannizzo*,* V.-T. Pham*,* F. Mourik, C. Bressler*,* M. Chergui*, J. Am. Chem. Soc.* **2007***, 129,* 8199-8206*;* c) *S.* Dick*, Z. Kristallogr. New Cryst. Struct.* **1998***, 213,* 356.
[13] a) I.-G. Filippova, A. Simonov, M. Gdanets, V. Stavila, *Journal of Structural Chemistry*, **2005**, *46,* 1095-1098*;* b) K. Teramoto, T. Kawasaki, T. Nishide, Y. Ikeda, *Acta Cryst.* **2015**, E*71*, m8–m9*;* c) T. Ohshita, A. Tsukamoto, M. Senna, *Phys. stat. sol.(a)*, **2004**, *201*, 762-768; d) Y. Umemura, Y. Minai, , T. Tominaga, *J. Phys. Chem. B*, **1999**, *103*, 647-652.
[14] a) P. Gütlich, A. Hauser, H. Spiering, *Angew. Chem. Int. Ed.* **1994**, *33*, 2024-2054; b) P. Gütlich, A. Hauser, *Coord. Chem. Rev.* **1990**, *97*, 1-22; c) P. Guionneau, Crystallography and Spin-crossover. A view of Breathing Materials *Dalton Trans.* **2014**, *43*, 382-393.
[15] a) L. Bénisvy, J.-C. Chottard, J. Marrot, Y. Li, *Eur. J. Inorg. Chem.* **2005**, 999-1002; b) M.-P. Batten, A.-J. Canty, K.-J. Cavell, T. Rüther, B.-W. Skelton, A.-H. White, *Acta Crystallogr.* **2004***, C60,* m316-m319; c) P.-C. Bruijnincx, I.-L. Buurmans, Y. Huang, G.; Juhász, M. Viciano-Chumillas, M. Quesada, J. Reedijk, M. Lutz, A.-L. Spek, E. Münck, E.-L. Bominaar, R.-J. Klein Gebbink, *Inorg. Chem*. **2011***, 50,* 9243-9255*.*
[16] a) A. Scheja, D. Baabe, D. Menzel, C. Pietzonka, P. Schweyen, M. Bröring, *Chem.–Eur. J.* **2015***, 21,* 14196-14204; b) J.-S. Pap, B. Kripli, M. Giorgi, J. Kaizer, G. Speier, *Transition Met. Chem.* **2011**, *36*, 481-487; c) J.-S. Pap, V. Bányai, D.-S. Szilvási, J. Kaizer, G. Speier, M. Giorgi, *Inorg. Chem. Commun.* **2011**, *14*, 1767-1772; d) J.-S. Pap, B. Kripli, V. Bányai, M. Giorgi, L. Korecz, T. Gajda, D. Arus, J. Kaizer, G. Speier, *Inorg. Chim. Acta*. **2011**, *376*, 158-169.
[17] S. Alvarez, P. Alemany, D. Casanova, J. Cirera, M. Llunell, D. Avnir, *Coord. Chem. Rev.* **2005**, *249*, 1693-1708.
[18] a) D. Casanova, J. Cirera, M. Llunell, P. Alemany, D. Avnir, S. Alvarez, *J. Am. Chem. Soc.* **2004**, *126*, 1755-1763; (b) J. Cirera, E. Ruiz, S. Alvarez, *Organometallics,* **2005**, *24*, 1556-1562.
[19] a) R.-L. Jaffe, G.-D. Smith, *J. Chem. Phys.* **1996**, *105*, 2780-2788; b) C. Janiak*,* S. Temizdemir, S. Dechert, W. Deck, F. Girgsdies, J. Heinze, M.-J. Kolm, T.-G. Scharmann, O.-M. Zipffel, *Eur*. *J. Inorg*. *Chem*. **2000**, 1229-1241; c) V.-B. Medakovic´, M.-K. Milc˘ic´, G.-A. Bogdanovic´, S.-D. Zaric´, *J. Inorg. Biochem.* **2004**, *98*, 1867–1873; d) J.-M. Sexton, A.-A. Elliott, A.-L. Steber, S.-A. Peebles, R.-A. Peebles, J.-L. Neill, M.-T. Muckle, B.-H. Pate, *Phys. Chem. Chem. Phys.* **2010,** *12,* 14263-14270.
[20] P. Hobza*,* H.-L. Selzle, E.-W. Schlag, *Chem. Rev.* **1994**, *94*, 1767-1785.
[21] a) N. N. L. Madhavi, G.-R. Desiraju, A.-K. Katz, H.-L. Carrell, A. Nangia, *Chem. Commun.* **1997**, *0*, 1953-1954; b) H.-C. Weiss*,* D. Blaser, R. Boese, B.-M. Doughan, M.-M. Haley, *Chem. Commun.* **1997**, *0*, 1703-1704; c) T. Steiner, M. Tamm, B. Lutz, J. van der Maas, *Chem. Commun.* **1996**, *0*, 1127-1128; d)*,* P.-L. Anelli, P.-R. Ashton, R. Ballardini, V. Balzani, M. Delgado, M.-T. Gandolfi, T.-T. Goodnow, A.-E. Kaifer, D Philip, *J. Am. Chem. Soc*. **1992**, *114,* 193.
[22] J.A. Réal, M.-C. Muñoz*,* E. Andrès, T. Granier, B. Gallois, *Inorg. Chem*. **1994**, *33*, 3587-3594.
[23] C.-P. Slichter*,* H.-G. Drickamer, *J. Chem*. *Phys*. **1972***,* 2142-2160.
[24] J.-P. Tuchagues, A. Bousseksou, G. Molnár, J.-J. McGarvey, F. Varret, in *Spin Crossover in Transition Metal Compounds, Top. Curr. Chem.,* vol. 235, (Eds: P. Gütlich, H.A. Goodwin) Springer-Verlag, **2004**, p. 85.
[25] G. Molnár, V. Niel, A.-B. Gaspar, J.-A. Real, A. Zwick, A. Bousseksou, J.-J. McGarvey, *J. Phys. Chem.* **2002**, B 106, 9701-9707.
[26] a) K.-S. Kumar, I. Salitros, B. Heinrich, O. Fuhr, M.-A. Ruben, *Mat. Chem*. **2015**, *3*, 11635-11644; b) T. Nakamoto, Z.-C. Tan, M. Sorai, *Inorg. Chem.* **2001**, *40*, 3805-3809.
[27] a) H.-S. Scott, T.-M. Ross, N.-F. Chilton, I.-A. Gass, B. Moubaraki, G. Chastanet, N. Paradis, J.-F. Létard, K.-R. Vignesh, G. Rajaraman, S.-R. Batten, K. Murray, *Dalton Trans*. **2013**, *42*, 16494-16509; b) V. Martínez, A.-B. Gaspar, M.-C. Muñoz, G.-V. Bukin, G. Levchenko, J.-A. Real, *Chem. Eur. J.* **2009,** *15*, 10960-10971.
[28] H. Petzold, P. Djomgoue, G. Hörner, J.-M. Speck, T. Rüffer, D. Schaarschmidt, *Dalton Trans.* **2016**, *45*, 13798-13809.
[29] S. De, J.-R. Jiménez, Y. Li, L.-M. Chamoreau, A. Flambard, Y. Journaux, A. Bousseksou, R. Lescouëzec, *RSC Adv.* **2016**, *6*, 17456- 17459.
[30] a) P. Roquette, A. Maronna, M. Reinmuth, E. Kaifer, M. Enders, H.-J. Himmel, *Inorg*. *Chem*. **2011***, 50,* 1942-1955; b) T.-E. Machonkin, W.-M. Westler, J.-L. Markley, *Inorg*. *Chem*. **2005***, 44,* 779-797; c) I. Bertini, C. Luccinat, *Coord. Chem. Rev*. **1996***, 150,* 77-110.
[31] J. Keeler in *Understanding NMR Spectroscopy* (2nd ed.), *Wiley,* **2010**, 274.
[32] a) A. Donaire, J. Salgado, H.-R. Jimenez, J.-M. Moratal, in *Nuclear Magnetic Resonance of Paramagnetic Molecules* (Eds.: G.-N. La Mar) Kluwer Academic Publishers, **1995**, 213; b) Z. Wang, Q. JR. Lawrence in *Nuclear Magnetic Resonance of Paramagnetic Molecules* (Eds.: G.-N. La Mar) Kluwer Academic Publishers. **1995**, 193.
[33] C. Belle, C. Bougault, M.-T. Averbuch, A. Durif, J.-L. Pierre, J.-M. Latour, L. Le Pape, *J. Am. Chem. Soc*. **2001**, *123*, 8053-8066.
[34] R.J. Kurland, B. R. McGarvey, *J. Mag. Res.* **1970**, *2*, 286-301.
[35] a) L. Banci, I. Bertini, C. Luchinat, R. Pierattelli, N.-V. Shokhirev, F.-A. Walker, *J. Am. Chem. Soc.* **1998**, *120*, 8472-8479; b) D.-L. Turner, *Eur. J. Biochem.* **1993***, 211*, 563-568.
[36] B. Weber, F.-A. Walker, *Inorg*. *Chem*. **2007**, *46*, 6794-6803*.*
[37] J.-P. Jesson in *NMR of Paramagnetic Molecules* (Eds.: G.-N. La Mar, W.-D. Horrocks, R.-H. Holm), Academic Press: New York. **1973**.
[38] a) F.-M. Regueiro, B. Bensenane, E. Ruscsák, D. Esteban-Gómez, L.-J. Charbonnière, G. Tircsó, I. Tóth, A. de Blas, T. Rodríguez-Blas, C. Platas-Iglesias, *Inorg. Chem*. **2011***, 50,* 4125-4141*;* b) M. Purgel, Z. Baranyai, A. de Blas, T. Rodríguez-Blas, I. Bányai, C. Platas-Iglesias, I. Tóth, *Inorg*. *Chem*. **2010***, 49*, 4370-4382; c)*,* D.-J. Press, Nicole M R. Mcneil*,* A. Rauk*,* T.-G. Back *J. Org. Chem.* **2012,** *77,* 9268-9276*.*
[39] The evaporation of the solvent above 350 K prevents the study at higher temperature.
[40] W. Klaui, W. Eberspach, P. Gütlich, *Inorg. Chem*. **1987**, *26*, 3977-3982.
[41] a) A. Flambard, F.-H. Köhler, R. Lescouëzec, B. Revel, *Chem.–Eur. J.* **2011**, *41,* 11567-11575; b) A. Flambard, F.-H. Köhler, R. Lescouëzec, *Angew. Chem. Int. Ed. **2009**, 48*, 1673-1676.
[42] a) R.-K. Wilson, S. Brooker, *Dalton Trans*. **2013***, 42,* 12075-12078; b) S. Heider, H. Petzold, G. Teucher, *Eur*. *J. Inorg*. *Chem*. **2013**, 2382-2388.
[43] a) S.-K. Sur, Measurement of Magnetic Susceptibility and Magnetic Moment of Paramagnetic Molecules in Solution by High-field Fourier Transform NMR Spectroscopy *J. Mag*. *Res*. **1989***, 82,* 169; b) D.-F. Evans, *J. Chem. Soc*. **1959**, 2003-2005.
[44] R.-C. Weast, M.-J. Astle, W.-H. Beyer in *Handbook of Chemistry and Physics*, CRC Press, *64 edn*. **1983**.
[45] G.-A. Bain*,* J.-F. Berry, Diamagnetic Corrections and Pascal's Constants *J. Chem. Educ*. **2008***, 85,* 532-536*.*
[46] C.-P. Slichter*,* H.-G. Drickamer, *J. Chem*. *Phys.* **1972***,* 2142-2160
[47] I. Bertini, P. Turano, A.-J. Vila, *Chem. Rev.* **1993**, *93*, 2833-2932.
[48] M. Reiher, O.Salomon, B.A.Hess, *Theor. Chem. Acc.* **2001**, *107*, 48-55.
[49] M. J. Swart, M. *J. Chem. Theory Comput.* **2008**, *4*, 2057

[50] D.N. Bowman, E. Jakubikova *Inorg. Chem.* **2012**, *51*, 6011-19
[51] S.J. Grimme, *Comput. Chem.* **2006**, *27*, 1787-99.
[52] K.P. Kepp, *Coord. Chem. Rev.* **2013**, *257*, 196-209
[53] G.R. Desiraju, T. Steiner, *The Weak Hydrogen bond in Structural Chemistry and Biology* , **1999**, Oxford University Press
[54] a) J. Tomashi, B. Mennucci, R. Cammi, *Chem. Rev.* **2005**, *105*, 2999-3094; b) G.-R. Desiraju, T. Steiner in *The Weak Hydrogen bond in Structural Chemistry and Biology*, **1999**, Oxford University Press.
[50] G.-M. Sheldrick, *Acta Cryst. A* **2008**, *64*, 112-122.
[51] a) P. Lucas, N. El Mehdi, H.-A. Ho, D. Bélanger, L. Breau, *Synthesis.* **2000***, 9,* 1253-1258*;* b) N. Braussaud*,* T. Ruther, J.-C. Kingsley, B.-W. Skelton, A.-H. White, *Synthesis*. **2001***, 4*, 626-632.
[52] L. Peters, F.-M. Tepedino, T. Haas, W.-F. Heinemann, M. Wolf, N. Burzlaff, *Inorg. Chim. Acta.* **2011***, 374,* 392-405*.*
[53] A. Altomare, G. Cascarano, C. Giacovazzo, A. Guagliardi, *J. Appl. Cryst.* **1993**, *26*, 343-350.
[54] L. Palatinus, G. Chapuis, *J. Appl. Cryst.* **2007**, *40*, 786-790.
[55] L.-J. Farrugia, *J. Appl. Cryst.* **1999**, *32*, 837-838.
[56] P.-W. Betteridge, J.-R. Carruthers, R.-I. Cooper, K. Prout, D.-J. Watkin, *J. Appl. Cryst.* **2003**, *36*, 1487.
[57] F. Jensen in *Introduction to Computational Chemistry*, *2nd Ed*, John Wiley & Sons Ltd, **2006**.
[58] Gaussian 09, Revision A.02, M.-J. Frisch, G.-W. Trucks, H.-B. Schlegel, G.-E. Scuseria, M.-A. Robb, J.-R. Cheeseman, G. Scalmani, V. Barone, G.-A. Petersson, H. Nakatsuji, X. Li, M. Caricato, A. Marenich, J. Bloino, B.-G. Janesko, R. Gomperts, B. Mennucci, H.-P. Hratchian, J.-V. Ortiz, A.-F. Izmaylov, J.-L. Sonnenberg, D. Williams-Young, F. Ding, F. Lipparini, F. Egidi, J. Goings, B. Peng, A. Petrone, T. Henderson, D. Ranasinghe, V.-G. Zakrzewski, J. Gao, N. Rega, G. Zheng, W. Liang, M. Hada, M. Ehara, K. Toyota, R. Fukuda, J. Hasegawa, M. Ishida, T. Nakajima, Y. Honda, O. Kitao, H. Nakai, T. Vreven, K. Throssell, J.-A. Montgomery, Jr., J.-E. Peralta, F. Ogliaro, M. Bearpark, J.-J. Heyd, E. Brothers, K.-N. Kudin, V.-N. Staroverov, T. Keith, R. Kobayashi, J. Normand, K. Raghavachari, A. Rendell, J.-C. Burant, S.-S. Iyengar, J. Tomasi, M. Cossi, J.-M. Millam, M. Klene, C. Adamo, R. Cammi, J.-W. Ochterski, R.-L. Martin, K. Morokuma, O. Farkas, J.-B. Foresman, D.-J. Fox, Gaussian, Inc., Wallingford CT, **2016**.
[59] F. Neese in *ORCA*, *An ab initio, DFT and Semiempirical Electronic Structure Package*, Version *3.0*, Institut für Physikalische und Theoretische Chemie, Universität Bonn, Bonn, Germany, **2010**; F. Neese, *The ORCA program system*. Wiley Interdiscip. Rev.: *Comput. Mol. Sci.* **2012**, *2*, 73.
[60] A.-D. Becke, *Phys. Rev.* A **1988**, *38*, 3098-3100.
[61] (a) C. Lee, W. Yang, R.-G. Parr, *Phys. Rev. B* **1988**, *37*, 785-789; b) B. Miehlich, A. Savin, H. Stoll, H. Preuss, *Chem. Phys. Lett.* **1989**, *157*, 200-206.
[62] a) A. Schafer, H. Horn, R. Ahlrichs *J. Chem. Phys.* **1992**, *97*, 2571-2577; b) A. Schafer, C. Huber, R. Ahlrichs, *J. Chem. Phys.* **1994**, *100*, 5829-5835.
[63] V.-A. Rassolov, J.-A. Pople, M.-A. Ratner, T.-L. Windus, *J. Chem. Phys.* **1998**, *109*, 1223-1229.
[64] P.-J. Hay, W.-R. Wadt *J. Chem. Phys.* **1985**, *82*, 299-310.
[65] M. Swart, *J. Chem. Theory Comput.* **2008**, *4*, 2057-2066.